

# **Highly Preheated Combustion Air System with/without Oxygen Enrichment for Metal Processing Furnaces**

AWARD # :: DE-FC36-02ID14348

## **FINAL TECHNICAL REPORT**

(09/01/2002 to 12/31/2006)

*Prepared by*

Arvind Atreya

Department of Mechanical Engineering  
The University of Michigan  
Ann Arbor, MI 48109-2125

*for*

**Dr. Bill Prymak**

DOE Project Officer, Golden Field Office,  
U.S. Department of Energy  
1617 Cole Boulevard, Golden, CO 80401

## FINAL TECHNICAL REPORT

**Project Title:** Highly Preheated Combustion Air System with/without Oxygen Enrichment for Metal Processing Furnaces.

**Covering Period:** 09/01/2002 to 12/31/2006

**Date of Report:** December 4, 2006

**Recipient:** **State of Michigan**  
Energy Office  
P.O. Box 30221  
Lansing, Michigan 48909

**Award Number:** DE-FC36-02ID14348

**Contact(s):**  
*Principal Investigator:* **John H. Sarver**, Energy Office, P.O. Box 30221, Lansing, Michigan 48909, Phone: 517/241-6224, Fax: 517/241-6229, Email: [jhsarve@michigan.gov](mailto:jhsarve@michigan.gov)

*Invoice Contact:* **Terri J. Eklund**, CIS, Financial Services, P.O. Box 30004, Lansing, MI 48909, Phone: 517/241-1668; Fax: 517/373-3621; Email: [tjeklun@michigan.gov](mailto:tjeklun@michigan.gov)

**Subcontractor:** University of Michigan, Department of Mechanical Engineering  
2350 Hayward Street, Ann Arbor, MI 48109-1225.

*Point of Contact:* **Dr. Arvind Atreya**, 2158 G.G. Brown Bldg. Email: [aatreya@umich.edu](mailto:aatreya@umich.edu)  
Phone: 734/647-4970; Fax: 734/647-3170.

**Other Partners:** N/A

**DOE Project Officer:** **Dr. Bill Prymak**, U.S. Department of Energy, Golden Field Office, 1617 Cole Boulevard, Golden, CO 80401, Phone: (303) 275-4931; Fax: (303) 275-4753; Email: [bill.prymak@go.doe.gov](mailto:bill.prymak@go.doe.gov)  
**Dr. Robert Gemmer**, Combustion Program, Office of Industrial Technologies, Energy Efficiency and Renewable Energy, EE-2F, Tel: 202-586-5885, Fax: 202-586-9234, Email: [bob.gemmer@ee.doe.gov](mailto:bob.gemmer@ee.doe.gov)

## PROJECT SUMMARY

**Project Objective:** The objective of this project was to develop and demonstrate a high temperature natural gas furnace that can operate with/without oxygen enrichment to significantly improve energy efficiency and reduce emissions. A laboratory-scale (5ft diameter & 8ft tall) furnace was constructed and tested. This report demonstrates the efficiency and pollutant prevention capabilities of this laboratory-scale test furnace. The project also developed optical detection technology to control the furnace output.

**Technical barrier(s) addressed:**

- (i) Flame radiation increase to decrease flame temperature to reduce NO<sub>x</sub>, and increase furnace productivity,
- (ii) Capture exhaust gas enthalpy to increase efficiency,
- (iii) Use of oxygen-enriched air without increasing NO<sub>x</sub> to decrease fuel consumption,
- (iv) Use of low calorific value fuel,
- (v) Oxygen-free atmosphere within the furnace to prevent metal oxidation,
- (vi) Multi-fuel capability, and
- (vii) Improved turn-down ratios.

**Project Pathway  
Adopted:**

This project developed furnace technology to significantly reduce energy consumption and emissions while improving productivity. While wasted flue gas enthalpy was not captured due to the laboratory furnace constraints, it can easily be captured in practice to highly preheat the incoming O<sub>2</sub> or O<sub>2</sub>-enriched air and fuel. Other than this aspect, rest of the goals were achieved. Internal flue gas recirculation was used to significantly dilute and heat the fuel and oxidizer before burning to decrease NO<sub>x</sub> production and increase heat flux uniformity within the furnace. A novel configuration was successfully tested where recirculation of combustion products and intense flame radiation were employed to reduce the flame temperatures and thus thermal NO. It utilizes buoyant recirculation and mixing of combustion products to reduce fuel and oxidizer concentrations and to increase the residence time of radiating combustion products. Nearly homogeneous burning is made to occur in distributed reaction zones under slightly rich conditions that enable increasing the flame radiation and also promote NO reburn. The resulting high & uniform heat flux enables an increase in the furnace productivity or a decrease in size and cost. This concept is equally applicable to many of the nation's most energy-intensive industries and water-tube boilers used for power production.

**Critical Technical Milestones Accomplished:**

- A small-scale furnace was designed, constructed and tested based on the above concepts. Measurements in this furnace unequivocally show that the above concepts can be successfully employed by industry. Due to the constraints imposed by the University on laboratory testing, we were unable to preheat the fuel and air and operate the furnace above 1000C. However, this can be easily accomplished in industry.
- We also modified a 3-D transient fluids code developed by NIST for fire applications to simulate mixing and combustion in the furnace. These numerical simulations show excellent agreement with the experiments and will be used to guide the full-scale implementation.
- Inexpensive visible and infrared detectors have been developed as intelligent furnace control devices. These detectors have been tested in a jet flame for implementation in an actual furnace.
- The real success of the furnace depends on adoption by the industry. Consequently, we established an Industrial Advisory Group (IAG) to guide

us during the furnace development phase. The IAG is very pleased with the laboratory-scale furnace results and the concept.

### **PROJECT ACCOMPLISHMENTS:**

**Furnace Design:** This involved conducting water experiments and numerical calculations to determine fuel and air injector locations and the furnace height required for dilution of fuel and air with burned gases and then mixing with each other. We also numerically estimated the expected temperatures and pollutant concentrations.

**Furnace Construction:** This involved selecting the right materials and a characteristic size and geometry to represent a large-scale furnace.

**Furnace Instrumentation for Measurements:** The furnace was instrumented for global measurements of fuel and air flow and flame radiation (using photodiodes, total heat flux calorimeters, visible and infrared cameras). Local measurements at several radial and axial locations were made of temperature with thermocouples and species with gas analysis equipment that measured CO<sub>2</sub>, H<sub>2</sub>O, O<sub>2</sub>, CO, HC and NO<sub>x</sub>.

**Developing Furnace Controls:** This involved selecting detector and filter combinations, calibrating them to interpret the measured radiation and testing them in a jet flame. This was completed and detectors for measuring CO<sub>2</sub>, H<sub>2</sub>O, hydrocarbons and soot radiation were developed. These detectors are non-intrusive and can be used for any industrial furnace.

**Industrial Advisory Group meetings:** Three such meetings were held during summers of 2003, 2004 & 2005 at Michigan provide program review, technical evaluation & direction for the project.

### **Student Graduated from the project:**

Ph.D. students graduated: (i) Ms. Tershia Pinder (March, 2006), (ii) Mr. Hyoseok Lee (Dec. 2006).

MS Students graduated: (i) Mr. Shreyas Sirsi (Jan. 2007)

### **Experimental Results:**

We developed the experimental furnace shown in Figure 1. The overall dimensions of this furnace are: 5' diameter and 8' tall. Here we accomplished mixing and dilution as shown in Figure 2 before reacting. Technically it turns out that this is not an easy to obtain homogeneous mixing on a chemical scale. Thus, either mixing has to be fast or chemistry has to be slow. If mixing is fast ( $\tau_{mixing} < \tau_{chemical}$ ) or chemistry is slow, we get homogeneous combustion otherwise flames. It is important to realize that first mixing and dilution has to be accomplished with fuel and burnt gases and oxidizer and burnt gases and then mixing between diluted fuel and diluted oxidizer. The results of the experiments conducted are summarized below:

### **Experimental Furnace Characteristics**

- Internal exhaust gas recirculation,

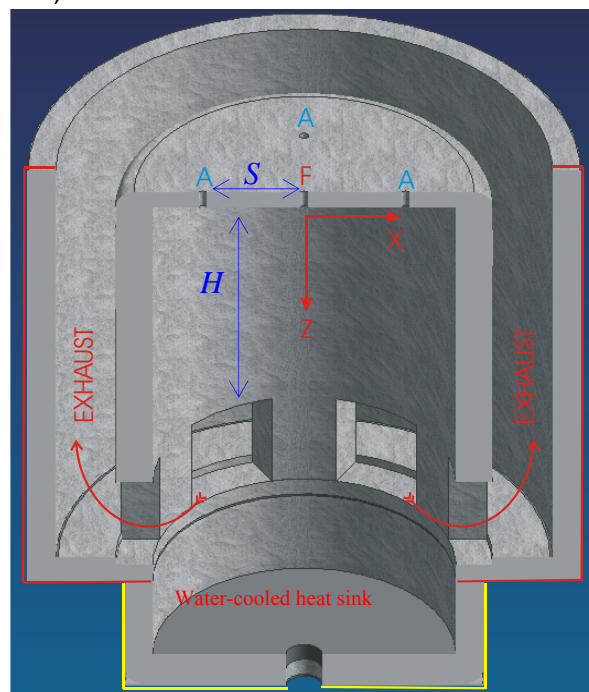


**Figure1: Cut-away view of the furnace showing the ceramic liners**

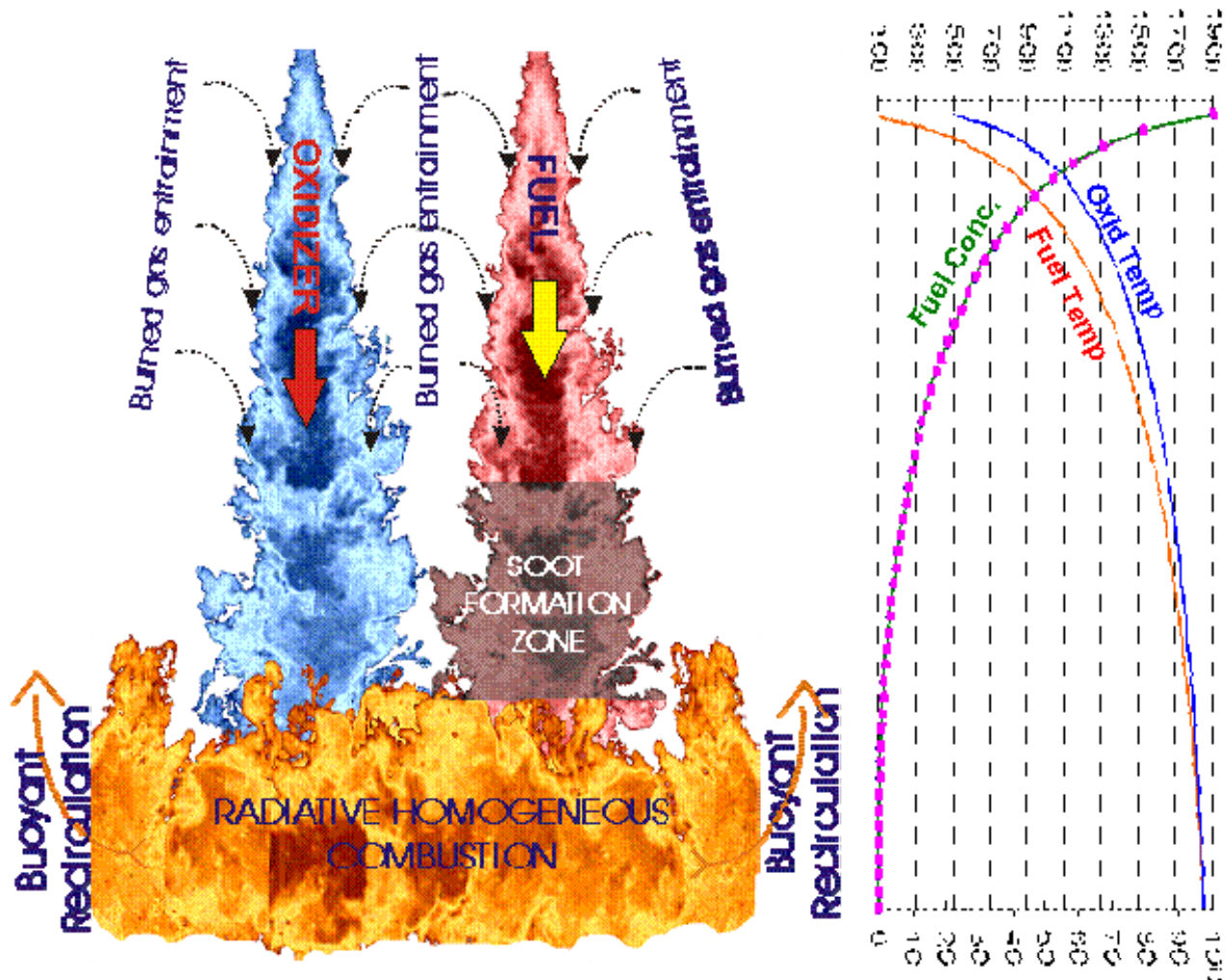


**Figure 2: A conceptual picture of what we want to happen in the furnace.**

- Fuel or oxidizer could not be preheated (University laboratory limitations)
- Downward evolving jet.
- Relatively large separation distance between fuel and air nozzle.
- Flame Froude number is about 0.32 which falls down to buoyancy affected jet.
- Enriched oxygen air flow (21, 30, 40%).
- Various nozzle diameters (to study the effect of momentum).
- While the fuel flow rate is fixed, parameters are changed by adjusting air flow condition.

#### **UV emission and conditions leading to HOMOGENEOUS COMBUSTION:**

Hasegawa's group [27<sup>th</sup> Symposium (International) on Combustion, 1998, 3135-3146] measured UV-visible emission spectra of the homogeneous combustion flame and showed that OH emission levels increases with the increase in the flame temperature. Plessing, T., Peters, N. and Wunning [27<sup>th</sup> Symposium (International) on Combustion, 1998, 3197-3204] measured planar LIF images of local distribution of the OH radical in the reaction zone and showed distributed and low OH concentration in the homogeneous combustion regime. OH band (281.1 nm, 306.4

nm) emission was captured by a UV photodiode and the UV emission data were used to evaluate the presence of the homogeneous combustion regime. The result was that UV emission was low and stable in the homogeneous combustion regime and it was high and fluctuated in the non-homogeneous combustion case. This UV emission was compared with visual images (flame colors such as yellow or blue) that validated the conclusion. Thus, UV emission detection can be used as criteria to identify the homogeneous combustion condition. In this work, homogeneous combustion operating parameter chart was made by varying the air nozzle diameter, oxygen concentration and equivalence ratio. Wunning and Hasegawa's homogeneous combustion operating condition charts takes care of temperature (furnace preheat temperature) and dilution rate ( $O_2\%$  + air nozzle diameter effect for our case). However, the operating condition charts for actual furnace application must include the information about geometric and flow condition. Thus, a new kind of operating chart using momentum versus  $d \times [O_2\%]$  is suggested here because momentum controls the mixing and dilution and  $d \times [O_2\%]$  controls the center-line  $O_2$  concentration.

The current furnace configuration resembles an inverted burner where the flames are usually unstable and easily extinguished and the ratio of inertia and buoyancy determines the stability of the reaction zone. However when the surrounding temperature is above the auto-ignition temperature, the flames are stable. It was found that depending on the amount of exhaust gas recirculation, the combustion was either in the diffusion flame mode (for small exhaust gas recirculation) or in the flameless mode (for high exhaust gas recirculation). It was also found that when enriched oxygen is used as oxidizer, even if there is large amount of dilution, the actual oxygen concentration can be high enough to initiate the diffusion flame mode. This is because of availability of sufficient oxygen to produce OH. Thus, in order to determine the stable homogeneous regime, the furnace experiments were performed for various momentum conditions by varying the air nozzle diameter, oxygen enrichment and equivalence ratio. Gas temperature at  $x = 6''$  and gas composition at  $y = 12''$  were measured for various  $Z$ . Figure 3 below shows the experimental measurement variables and geometry.

Two parameters are used to evaluate the effect of dilution, buoyancy and jet momentum based on the air injection parameters (the fuel nozzle diameter and the flow rate are kept constant): For a single non-reactive turbulent jet, the downstream concentration  $C(r, x)$  of the jet fluid is self-similar and given by:

$$C(r, x) = k \frac{C_0 d^*}{x - x_0} g\left(\frac{r}{x - x_0}\right),$$

where  $C_0$  is the jet exit concentration,  $d^*$  the momentum diameter of the nozzle exit and  $x_0$  the virtual origin of the jet flow. It is noted that the concentration itself is not affected by the jet exit velocity but it is a function of the jet exit concentration. Therefore, the local concentration of  $O_2$  is the function of  $X_{O_2}d$ .

To account for the effect of buoyancy, the ratio of inertia and buoyant forces is important. This can be represented by the Archimedes Number. However, by using experimental data of inlet jet temperature and average gas temperature in reaction chamber it is found to be roughly the same order of magnitude for most cases. Therefore, the inertia term, or the momentum flow term given by  $J = \dot{m}v$ , is the parameter that represents the jet flow. Note that the air nozzle diameter affects both the jet momentum flow and the oxygen concentration.

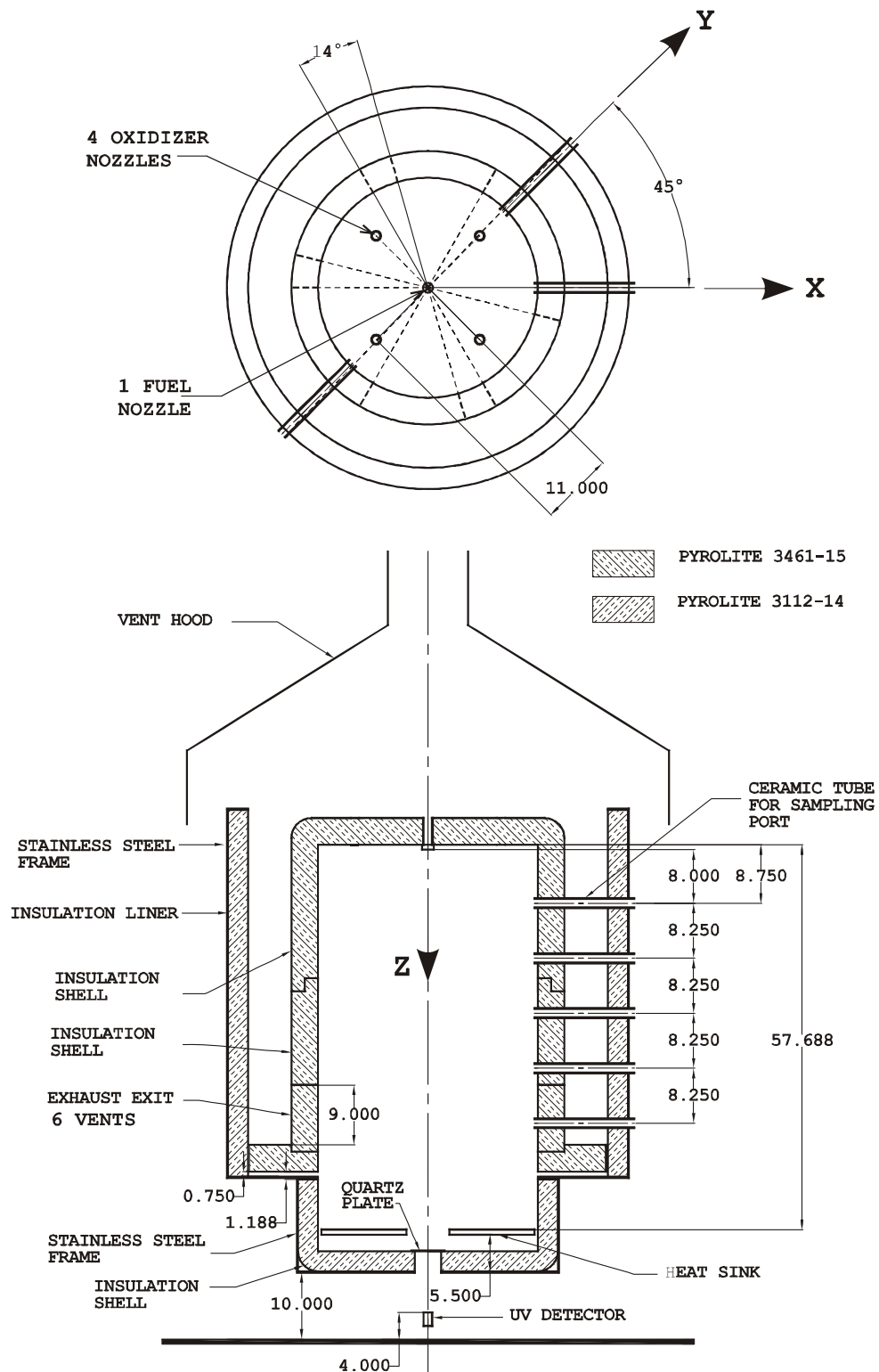


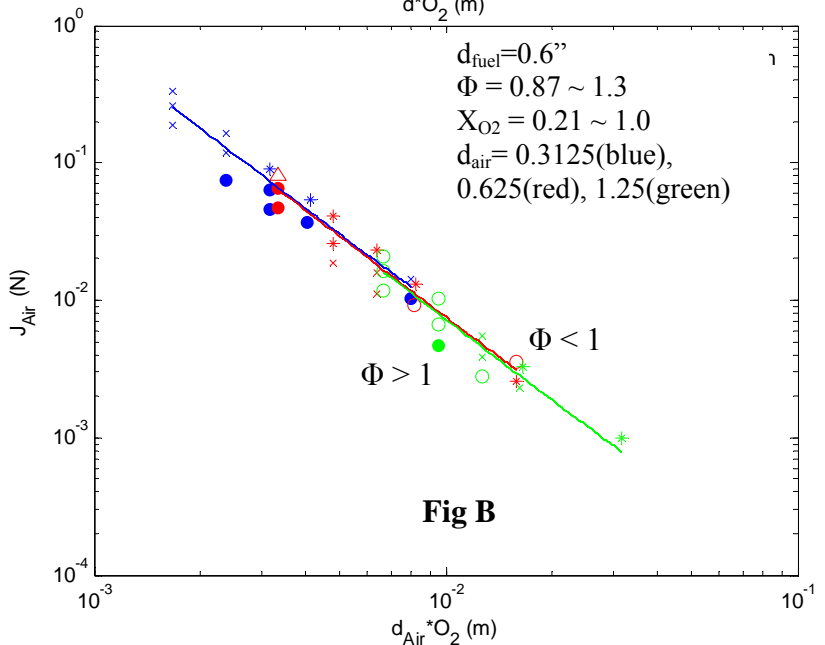
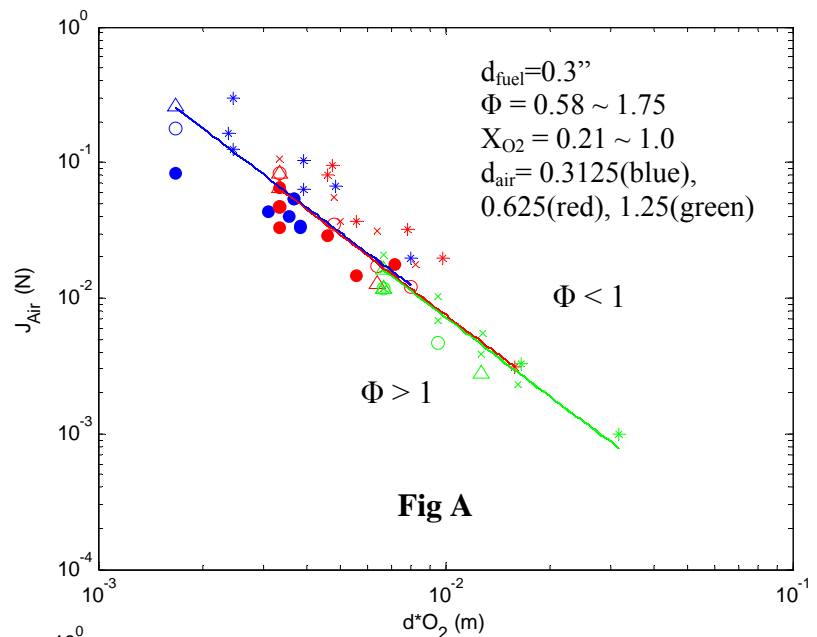
**Figure 3:** Schematic of the experimental furnace layout for measurements



By using two parameters,  $J_{air} = \dot{m}v[N]$  and  $\chi_{O_2} \cdot d_{air}[m]$ , the homogeneity for various conditions is plotted in Fig. A for fuel nozzle diameter 0.3 in and Fig. B for fuel nozzle diameter 0.6 in. Test range for searching these condition is  $\Phi = 0.58 \sim 1.75$ ,  $X_{O_2} = 0.21 \sim 1.0$  for fuel nozzle diameter 0.3", and  $\Phi = 0.87 \sim 1.3$ ,  $X_{O_2} = 0.21 \sim 1.0$  for fuel nozzle diameter 0.6". The abscissa represents the effective oxygen concentration  $X_{O_2} \cdot d$  and the ordinate represents air momentum  $J_{air}$ . The experiments were performed for three different diameter of air 0.3125(blue), 0.625(red), 1.25(green) for a fixed fuel flow rate of 2.95cfm. The lines for equivalence ratio = 1 have different value for each of the three cases, but they are roughly the same for our experimental range. The criterion used for judging the combustion homogeneity is: If either yellow or blue flames do not exist (visually), the reaction is identified as homogeneous. This criterion turns out to be equivalent to the OH criterion. In figures A & B, filled symbols represent homogeneous conditions, whereas, open symbols represent flames.

As seen in the figures, lean conditions tend to be in diffusion mode and rich conditions in homogeneous mode. Small air nozzle diameter satisfies the homogeneous condition for wide range of air momentum, whereas, the large air nozzle diameter satisfies the condition only for large air momentum. Over the scanning range, the gas measurements at  $y = 12''$  show that CO is high for the homogeneous case and NO is high for the diffusion flame case.

Examples of temperature profile at  $x = 6''$  are shown in figures C, D, and E for the change of equivalence ratio (Fig.C), change of oxygen concentration (Fig. D) and change of air nozzle diameter or momentum (Fig. E) respectively. Since fuel flow rate is fixed and only air flow rate adjusted for all cases, higher equivalence ratio or higher oxygen concentration means lower air momentum ratio. As seen in Fig. C and D, the peak temperature moves to upstream of the jet flow for





higher momentum if other parameters are fixed.

### Effect of Air Jet Nozzle

#### Diameter/Momentum:

- If the diameter of the air nozzle decreases the exit velocity increases for the same flow rate. Under these conditions, homogeneous combustion is obtained. This is because of enhanced mixing and dilution for the air jet at high velocities. From the characteristics of the jet concentration profile,  $[C \sim C_0(d/x)]$ , the larger the diameter of the air nozzle, more delayed the mixing and combustion and the high temperature region moves downstream [Fig. E].
- Generally lower NO and CO is obtained for smaller diameter of the air nozzle. From the above equation, the smaller the diameter, the smaller the concentration because the entrained mass of burned gases ' $m_e$ ' and hence the dilution increases according to the relation:

$$\frac{m_e}{m_0} \sim \left( \frac{\rho_\infty}{\rho_0} \right)^{1/2} \frac{x}{d}. \quad \text{For smaller}$$

diameter of the air nozzle, there is larger entrainment.

- It is difficult to achieve stable homogeneous combustion for small diameter air nozzle ( $d=0.3125$ ) because the temperature in the furnace falls due to the high velocity air jet – lot of excess nitrogen.
- On the other hand, it is difficult to achieve homogeneous combustion condition for the oxygen enriched case because of low flow momentum and air dilution. Thus, the nozzle diameter must be decreased or fuel rich condition should be used to slow down the chemistry.

### Effect of Oxygen Concentration

- If the oxygen concentration of the air jet decreases (both jet exit velocity and flow rate must increase to provide the same amount of oxygen for combustion), homogeneous combustion is obtained. This is both due to dilution caused by enhanced mixing and low initial concentration of oxygen. The lower oxygen concentration throughout the volume slows

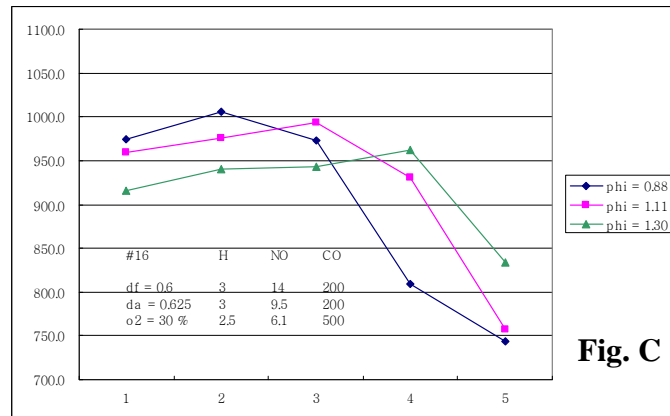


Fig. C

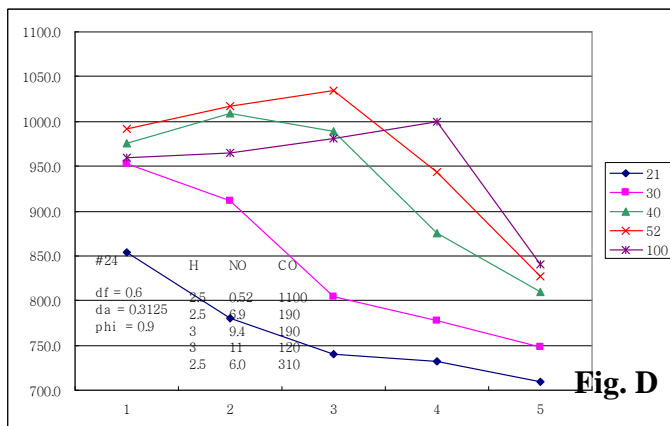


Fig. D

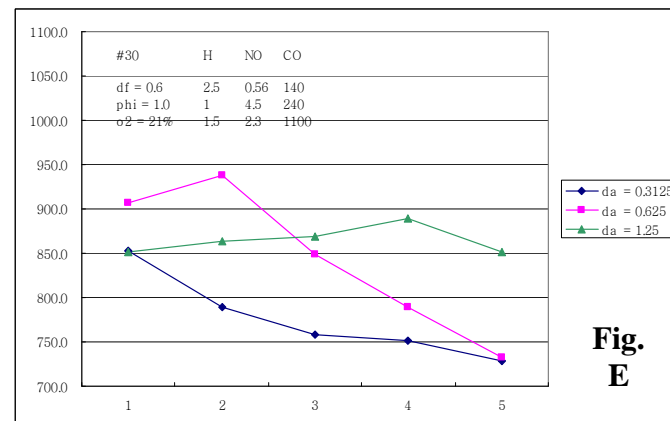


Fig. E

down the  $H_2-O_2$  chain branching reaction, preventing flames. For higher oxygen concentration, the high temperature region spreads downstream, Figure D.

### Effect of Equivalence Ratio

- If equivalence ratio increases (i.e. both air velocity and flow rate decreases for the same fuel flow rate), homogeneous combustion is obtained. The effect is for much the same reasons as the effect of oxygen above, except for increased oxidizer dilution due to higher momentum. However, the slow down in the chemical reaction rates is due to the same reasons. For higher equivalence ratio, the high temperature region spreads downstream, Figure C.
- For lean conditions, the oxygen mass flow rate and following air jet entrainment must be larger. The presence of excess oxygen for the lean case, promotes formation of flames. It is important to note that ‘H-atom’ can diffuse very fast to start the  $H_2-O_2$  chain branching reaction if oxygen can be found.
- For rich condition, generally homogeneous combustion is obtained, as well as, lower NO concentrations.

### NO and CO Concentrations

- NO concentration profile roughly follows temperature profile.
- For CO concentration, it is found that high CO concentration region moves with the high temperature region. By comparing with the local equivalence ratio profile, the CO concentration profile follows the same pattern and behavior. High CO regions correspond to rich regions. In order to reduce CO, the fuel should be diluted enough to be in the lean condition before it meets oxygen.
- The flame zone can be determined by CO concentration [Flamme, M., Energy Conversion and Management Vol. 42, pp. 1919-1935 (2001)]. If air nozzle diameter decreases or oxygen concentration of the air jet decreases, the flame turns to be in homogeneous combustion condition and the flame zone stays upstream. That is an advantage to reduce the size of the reaction chamber of the furnace.

Representative temperature and gas compositions distributions for the following cases are shown below:

Case	Fuel diameter	Air diameter	Oxygen concentration	Equivalence ratio
Fig. F	0.6 in	0.3125 in	30 %	1.28
Fig. G	0.6 in	0.625 in	21 %	1.0
Fig. H	0.6 in	1.25 i	21 %	1.0

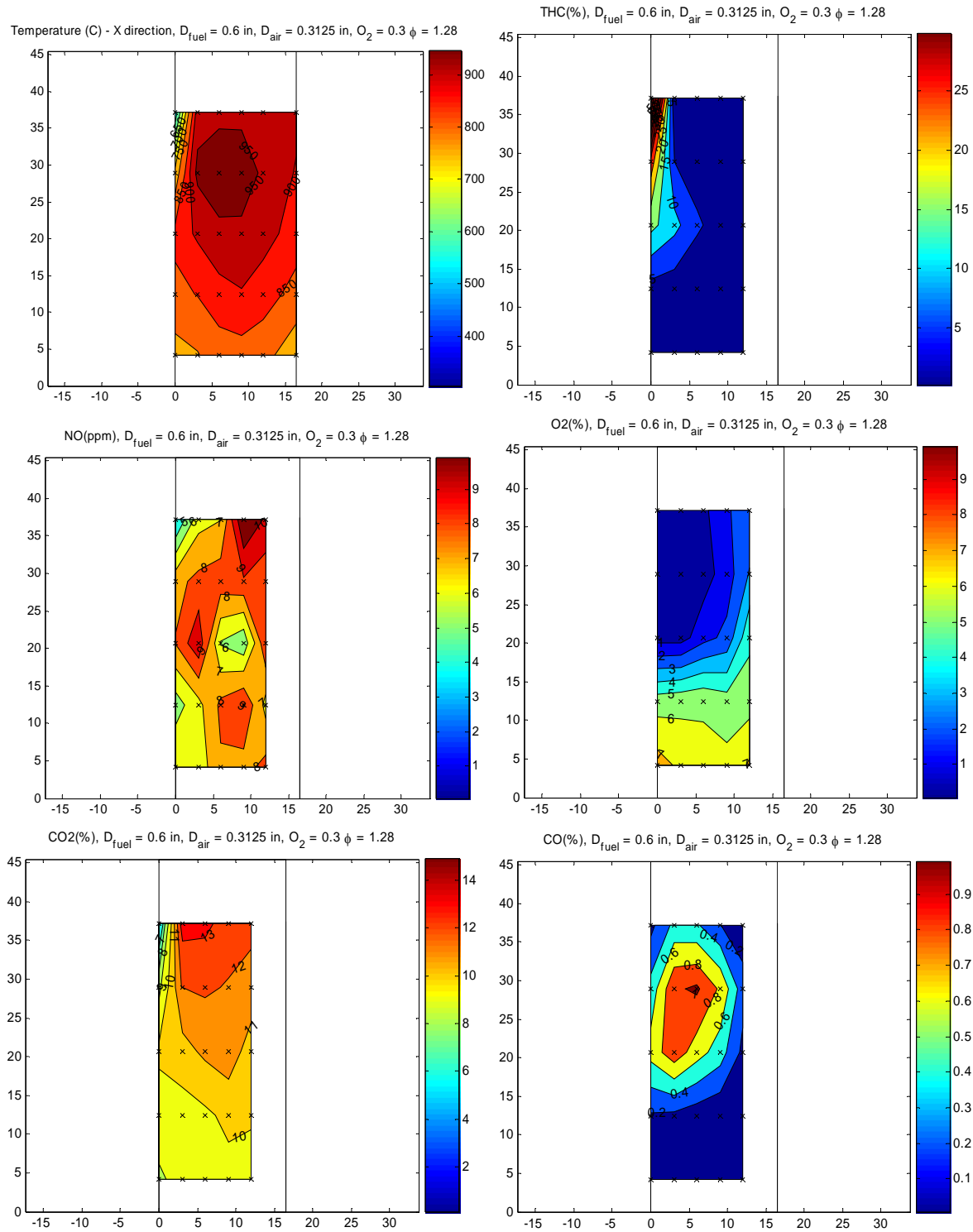


Fig. F

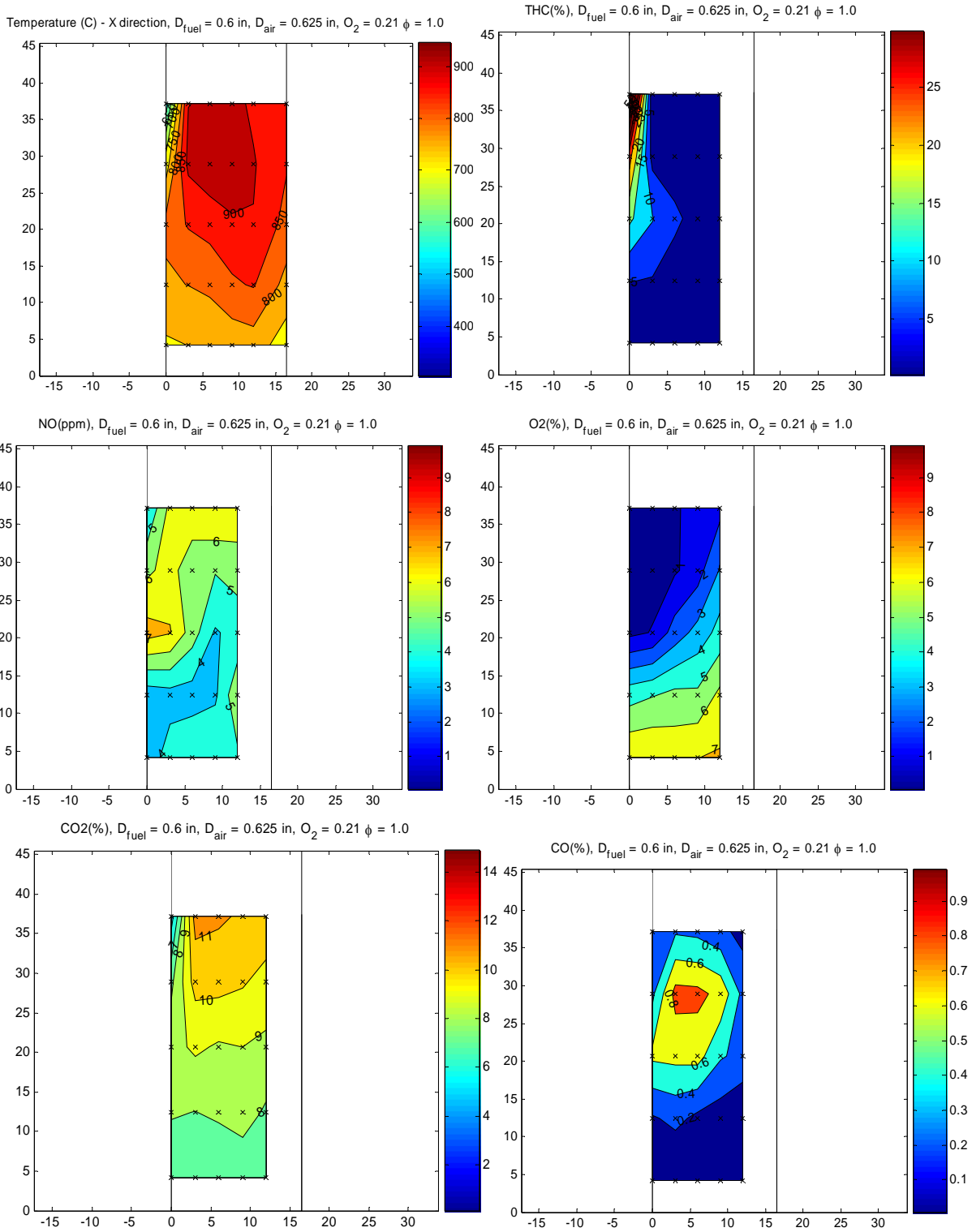


Fig. G

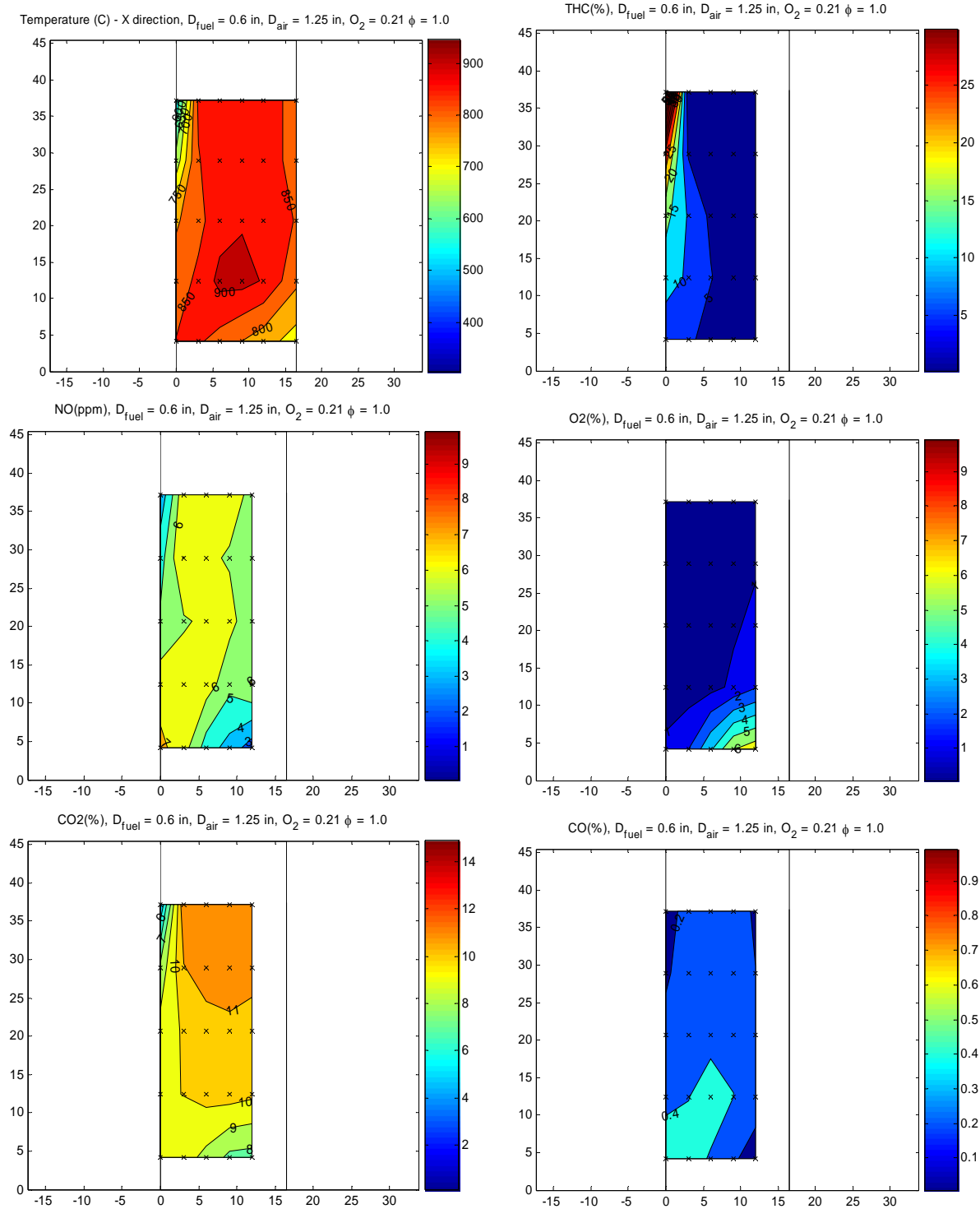


Fig. H

**Project Changes:**

No changes were made in the scope of the proposed work.

**Commercialization Potential, Plans, and Activities:**

The technology developed in this project is expected to be utilized by industries represented by the DOE Industries of the Future program. These are energy-intensive industries like aluminum, chemicals, glass, metal casting, pulp and paper, and steel. These industries are in dire need of energy efficient, low pollutant forming high temperature furnaces. This technology is also equally applicable to water-tube boilers used in power plants. Thus, we believe that the commercialization potential is high. Our Industrial Advisory Board has given us many suggestions in this regard. With the development of a working laboratory furnace, we also hope to convince industrial users to implement such a furnace for actual application with DOE help. The PI's SEN visits to Iron and Aluminum companies confirm that the present furnace is desperately needed in these companies.

Our Industrial Advisory Board wanted us to demonstrate the furnace technology in real application and show a cost-benefit analysis. To do this, we have been in touch with Mittal Steel in Burns Harbor. They are willing to modify an existing in-and-out production billet reheating furnace with this technology. However, the modification is expensive and Mittal Steel and University of Michigan jointly can not foot the bill. We have therefore written a proposal to DOE to help us demonstrate the furnace. The proposal was submitted to DOE under the Steel solicitation "DOE Collaborative Energy Efficiency Research in Iron-Making and Steel-Making – Funding Opportunity Number: DE-PS36-06GO96008." The proposal was entitled: *"Development and Full-Scale Demonstration of New Furnace Technology to Significantly Improve Energy Efficiency and Reduce Emissions in Steel Reheating Furnaces."* We await the outcome of this proposal for wide technology adoption. We would also have filed for the "Michigan 21<sup>st</sup> Century Jobs Fund" but Mittal Steel is an Indiana company. In summary, we are looking for funds to do a full-scale demonstration.

**Publications and Presentations:**

*With the graduation of Ms. Tershia Pinder, Mr. Hyoseok Lee & Mr. Shreyas Shri, several publications have resulted from this work and many more are yet to come. They are:*

1. S. J. Shin, H. S. Lee and A. Atreya, "A Study of Dilution and Mixing of Unconfined Multiple Turbulent Jets for Industrial Furnaces," 5th US Combustion Meeting, March 25-28, 2007.
2. Arvind Atreya, "A Novel Method of Waste Heat Recovery from High Temperature Furnaces," ACEEE Conference on Energy Efficiency in Industry, 2007.
3. Hyoseok Lee, "Experimental Study of Jet Mixing in a Mild Combustion Furnace," Ph.D. thesis, University of Michigan, Ann Arbor, expected 2007.
4. Atreya, A. "High Temperature Industrial Furnace Based on Radiative Homogeneous Combustion for Improved Efficiency and Reduced Emissions," TMS 2006 Annual Meeting, 2006.
5. T. Pinder, S. Sirsi, C. Brogan, and A. Atreya, "Effect of Fuel Concentration Fluctuations on Non-premixed Jet Flames," 2006 Technical Meeting of the Central States Section of The Combustion Institute, May, 2006.
6. T. Pinder, S. Sirsi, C. Brogan, A. Atreya, "An Experimental Investigation Of The Effect Of Velocity Fluctuations On Nonpremixed Buoyant Jet Flame," 31<sup>st</sup> International Combustion Symposium, The Combustion Institute, August, 2006.

7. T. Pinder, "Effect of Velocity and Fuel Concentration Fluctuations on Nonpremixed Jet Flames," Ph.D. thesis, University of Michigan, Ann Arbor, 2006.
8. H. Lee, S.J. Shin, T. Pinder, and A. Atreya, "Radiative Homogeneous Combustion for Improved Efficiency and Reduced Emissions," ACEEE Conference on Energy Efficiency in Industry, 2005.
9. Pinder, T and Atreya, A., "Optical Measurements of Radiative Emission to Monitor the Effect of Fuel Concentration Fluctuations on Nonpremixed Flames," Fourth Joint Meeting of the U.S. Section of the Combustion Institute, March 2005, Philadelphia, PA.
10. Pinder, T and Atreya, A., "An Experimental Investigation of the Effect of Fuel Concentration Fluctuations On Nonpremixed Jet Flames," Presented at the Thirtieth International Symposium on Combustion, July 2004, Chicago, IL.
11. H. S. Lee and A. Atreya, "Experiments and Simulations of Mixing of Aligned Multiple Fuel-Air Jets," Fourth Joint Meeting of the U.S. Section of the Combustion Institute, March 2004, Philadelphia, PA.
12. T. Pinder and A. Atreya, "An Experimental Investigation of the Effect of Fuel Concentration and Velocity Fluctuations on Nonpremixed Jet Flames," 2004 Technical Meeting of the Central States Section of The Combustion Institute, May, 2004.
13. A. Atreya and D. Everest, "Highly Preheated Combustion Air Furnace with Oxygen Enrichment for Metal Processing to Significantly Improve Energy Efficiency and Reduce Emissions," ACEEE Conference on Energy Efficiency in Industry, 2003.

#### **PATENTS**

14. Atreya, A., "A Method of Waste Heat Recovery from High Temperature Furnace Exhaust Gases," Pending, Ref. #: 2115-003464, 2006.
15. Atreya, A., "Furnace Having Increased Energy Efficiency and Reduced Pollutant Formation," U.S. Patent No. 7784-002187, 2004.



5<sup>th</sup> US Combustion Meeting  
Organized by the Western States Section of the Combustion Institute  
and Hosted by the University of California at San Diego  
March 25-28, 2006.

## A Study of Dilution and Mixing of Unconfined Multiple Turbulent Jets for Industrial Furnaces

*S. J. Shin, H. S. Lee and A. Atreya*

*Department of Mechanical Engineering, University of Michigan at Ann Arbor,  
MI48109, USA*

Multiple turbulent jet flames are widely employed in industrial furnaces. The flame pattern and emissions depend on the jet interaction and mixing. This paper presents an experimental and numerical investigation of the mixing characteristics and the resulting concentration fields in unconfined, non-reacting multiple turbulent jets. Experimentally, Planar Laser Induced Fluorescence (PLIF) was employed to study the effects of the Reynolds number, separation distance, and momentum ratio on jet interaction and mixing in three round collinear jets. The three jet configuration was chosen to represent a center fuel jet surrounded by two air jets. The experimental results are compared with predictions using the Fire Dynamics Simulator (FDS) developed by National Institute of Standards and Technology (NIST). The numerical results were found to be in good agreement with the experimental data. FDS is then used to test different jet configurations and will be used for simulating confined and reacting jets in furnaces. The results of this study show that greater dilution in the mean centerline concentration of the center jet occurred at lower separation distance due to enhanced jet interaction. Increasing the momentum of the side jets showed more dilution and better mixing as a result of increased entrainment of the ambient fluid. Extensive numerical studies in a representative five turbulent jet configuration with a center fuel jet surrounded by four oxidizer jets are presented. These provide fundamental guidelines for optimization of the control parameters, jet spacing, momentum ratio of fuel to oxidizer jet, for industrial furnaces with multiple turbulent jets.

### 1. Introduction

Multiple turbulent jet configurations are widely employed in many industrial applications such as a furnace, diesel engine and aircraft propulsion system. In most industrial furnaces, fuel and oxidant are injected with high momentum through a nozzle, orifice and diffuser. As a result, the flame pattern and emissions strongly depend on the jet interaction and mixing under this configuration. Therefore, it is very important to understand the mutual interaction of multiple jets from the practical point of view.

Recently, novel combustion technologies for significant energy saving and reducing pollutant emissions have been developed for industrial furnaces. These may be classified as the homogeneous combustion. Examples include, Flameless Oxidation (FLOX), High Temperature Air Combustion (HiTAC), and Moderate and Intense Low oxygen Dilution (MILD) that have been developed in Europe and Japan [32-35]. The essential conditions for achieving these combustion modes are direct and separate injection of fuel and oxidant with high momentum, and the high recirculation of hot exhaust products. Another important condition is that the fuel and oxidant should be sufficiently diluted by the surrounding fluid before they react. Thus, the

analysis of the interaction, mixing and dilution patterns between the separate jet flows is essential for understanding the homogeneous combustion process.

Although numerous works on a single turbulent jet are available in literature, very little investigations have been conducted on the flow structure and passive scalar transport of multiple jets due to the complicated characteristics of the multiple turbulent jets.

Krothapalli et al. [2] investigated the detailed structure of the flow field with an array of rectangular lobes. Raghunathan and Reid [3] showed that a multiple jet configuration with five nozzles have an advantage in terms of noise reduction without significant momentum reduction of the jet. Mostafa et al. [10] performed the experimental and numerical studies on three rectangular turbulent jets. In this work, the authors confirmed that there is a strong mutual entrainment and turbulent transport between jets. Theoretical approaches to parallel rectangular multiple jets were conducted by Chuang et al. with a kinetic theory of turbulence [7] and Wang et al. with the thin layer theory [11]. Experimental studies on twin round interacting jets were performed by Becker and Booth [1], Moustofa [8], and Okamoto et al. [4].

The co-flowing plane jets with different velocity and momentum ratio have been studied by Grandmaison et al. [5]. The effect of the nozzle spacing on jet interaction was studied by Wlezien et al. [6]. Manohar et al. [13] presented the experimental and numerical results of the interaction between multiple incompressible air jets. The authors found that the merge distance between jets increase for larger jet spacing and the entrainment is more enhanced under multiple jet configurations than a single jet. Yimer and Becker [12] investigated the strong-weak jet coupling for developing a new concept for low-NO<sub>x</sub> burners. They found that the point of jet confluence strongly depends on the jet separation distance and momentum ratio between jets.

The majority of these works were mainly focused on the behavior of the velocity flow field. Research on the fundamental aspects of passive scalar mixing such as the concentration field in multiple turbulent jets is very limited.

This study presents an experimental and numerical investigation of the mixing characteristics and the resulting concentration fields in unconfined, non-reacting multiple turbulent jets. Experimentally, Planar Laser Induced Fluorescence (PLIF) was employed to study the effects of the Reynolds number, separation distance, and momentum ratio on jet interaction and mixing in three round collinear jets. The experimental results are compared with predictions using the Fire Dynamics Simulator (FDS) developed by National Institute of Standards and Technology (NIST). In addition, extensive numerical studies in a representative five turbulent jet configuration with a center fuel jet surrounded by four oxidizer jets are presented. These provide fundamental guidelines for optimization of the control parameters, jet spacing, momentum ratio of fuel to oxidizer jet, for industrial furnaces with multiple turbulent jets.

## 2. Experimental apparatus and method

### 2.1. Experimental Setup

Figure 1 (a) shows the schematic of water reservoir and water jet supply unit. The large rectangular water reservoir 1.5×1.5 m wide and 1.0 m high contains quiescent fresh water 0.75 m deep. Three circular nozzles of 10.4 mm exit diameter are installed vertically below the water surface. They are aligned in series at distance  $S$  separated from each other, measured from the centers of the circular nozzles. The separation distance between the jets can be adjusted to 38.1,

57.2 and 76.2 mm, which equals 3.66, 5.50 and 7.33 times the jet diameter. The jet flows are injected downward from the nozzles into the water in reservoir.

The flow velocity from the nozzles is maintained nearly constant during the experiment by two water supply units with two tanks and pumps which are designed to keep water level constant in tank 2. The head from the water surface of the reservoir to the water surface in tank 2 is about 2 m. The center jet (often containing the dye to simulate the fuel) is driven by one unit and the two other jets are driven by the other unit together. To identify fluids from each jet, either one of the water supply units may contain fluorescent dye (Rhodamine WT). The dye is well dissolved in one of the water supply units to obtain a concentration of about 1.5 mg per 1 L of water.

To obtain the concentration profile, planar Laser Induced Fluorescence (PLIF) is used as flow visualization technique. Schematic of the PLIF system is illustrated in Figure 1 (b). Nd-YAG laser (Surelite I PIV 10 Hz, Continuum) having a wavelength of 532 nm and power of about 2 W is used as a light source and the laser is synchronized with the CCD camera (PIVCAM 10-30, TSI Inc.) having 1000×1016 resolution and 8 bit dynamic range. The pulsed laser beam passes through a pinhole to adjust the size and then passes through the cylindrical plano-concave lens which expands it vertically to a laser sheet. Finally by a slit the laser sheet is trimmed into a thin layer sheet about 1 mm wide.

The vertical laser sheet is adjusted to pass through the centerline of the aligned center of the three jet nozzles. When the jet containing the fluorescent dye is injected from the nozzle, the dye is excited by the laser light sheet to create the fluorescent image. The image is taken by the CCD camera. Laser pulse duration time is 6 ns, camera shutter exposure time is 255  $\mu$ s, and laser pulse repetition rate is 10 Hz. The resolution based on the camera setup is 0.64×0.64 mm per pixel.

## 2.2. Experimental Method

In this study, all the jet image data are averaged during 25s, i.e. 250 laser shots, after the flows turn to be steady and fully developed. Even though the data is averaged over time, there is still the possibility of instrumental noise. Specially, in case of the pulsed laser used in this experiment, the laser light intensity of shots varies randomly within in a range. While there is other instrumental noise involved together, the prediction of the proper noise level for each event and each pixel is indistinct. After series of calibration applications by the author, it was determined that the noise can be optimally removed by the convolution of 5×5 matrix.

The range of turbulent conditions in the experimental work was  $0.96 \times 10^4 < Re < 2.4 \times 10^4$ . The Reynolds number is calculated based on the nozzle diameter and the mean jet velocity of the flow exit. Water is used as a working fluid that has a Schmidt number,  $Sc > 600$  implying little diffusion-enhanced mixing. The turbulent jet is injected into the quiescent water with the same temperature. Since the density of the jet flow and the ambient fluid is the same, no buoyant effect is involved in these experiments.

While the pulsed laser light sheet passes vertically through the center of the aligned jets, the fluorescent dye is injected through the middle jet into the water reservoir. The fluorescent images are taken by the CCD camera synchronized with the laser pulse. In the beginning, the experimental setup and procedure is validated by measuring the concentration characteristics of turbulent single jet. The single jet was tested for four different jet exit velocities: 1.0, 1.5, 2.0 and 2.5 m/s. Corresponding Reynolds numbers were  $1.16 \times 10^4$ ,  $1.75 \times 10^4$ ,  $2.33 \times 10^4$ , and  $2.91 \times 10^4$ .

In order to investigate the effect of the separation distance and in particular to evaluate the effect of the side jets on the middle jet, three different separation distances,  $S/D = 3.66$ ,  $5.50$  and  $7.33$ , were tested. The effect of the momentum ratio between jets is investigated by changing the velocity of the jets while the diameter and flow rate of the jets are kept the same.

After performing the calibration procedure, mean concentration is obtained. In experimental studies, the measurements are made up to  $Z/D=50$  because of the spatial limitations. The coordinate system used in this experimental study is given in Figure 1 (c).

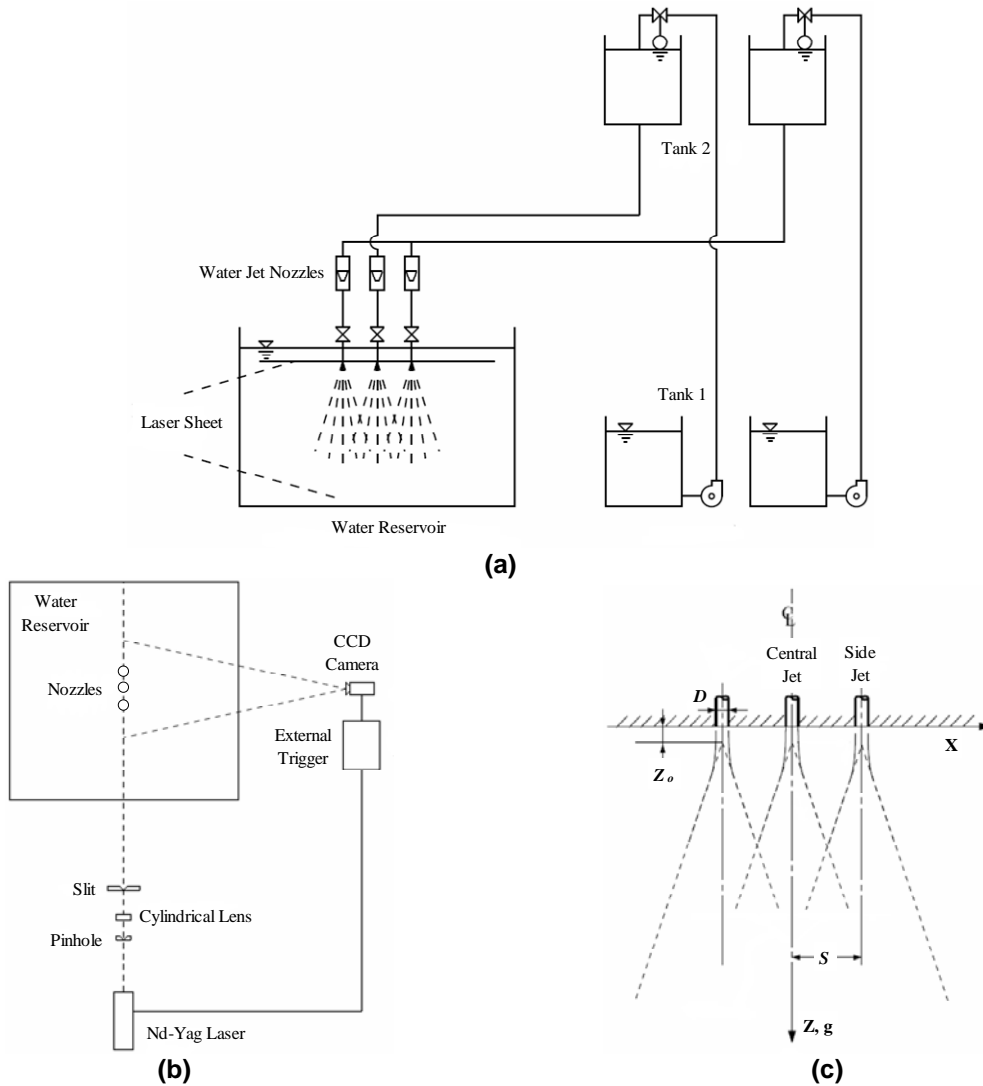


**Figure 1: Schematics of: (a) The water reservoir and water jet supply system (b) The PLIF system (c) The coordinate system nomenclature**

### 3. Numerical Simulation Method

Numerical simulations were performed by using the Fire Dynamics Simulator (FDS) developed at the National Institute of Standards and Technology (NIST) [36].

### 3.1. Governing equation

In the FDS code, the flow field is modeled by solving the conservation equations for mass, species, momentum and equation of state for the gas with low Mach number assumption. Under this assumption, the basic governing equations are simplified to,

$$\frac{\partial \rho}{\partial t} + \nabla \cdot \rho \mathbf{u} = 0 \quad (1)$$

$$\frac{\partial}{\partial t}(\rho Y_i) + \nabla \cdot \rho Y_i \mathbf{u} = \nabla \cdot \rho D_i \nabla Y_i + \dot{m}_i''' \quad (2)$$

$$\rho \left( \frac{\partial \mathbf{u}}{\partial t} + (\mathbf{u} \cdot \nabla) \mathbf{u} \right) + \nabla p = \rho \mathbf{g} + \mathbf{f} + \nabla \cdot \tau \quad (3)$$

$$p_o(t) = \rho TR \sum_i \frac{Y_i}{M_i} \quad (4)$$

Where,  $\mathbf{u} = (u, v, w)$  is the velocity field,  $\mathbf{f}$  is the external force on the fluid,  $\tau$  is the viscous stress tensor, and  $\dot{m}_i'''$  is the mass production rate of the  $i^{\text{th}}$  species per unit volume.

### 3.2. The turbulence model

The effect of the flow field turbulence is modeled using LES, in which the large scale eddies are computed directly and the sub-grid scale dissipative processes are modeled. To approximate the turbulent stress, the Smagorinsky model with a constant coefficient  $C_s$  is used everywhere in the flow field. In this model, the dynamic viscosity is defined at cell centers as,

$$\mu_{LES} = \rho (C_s \Delta)^2 \left( 2(\text{def} \mathbf{u}) \cdot (\text{def} \mathbf{u}) - \frac{2}{3} (\nabla \cdot \mathbf{u})^2 \right)^{\frac{1}{2}} \quad (5)$$

Where,  $C_s$  is the Smagorinsky constant, Grid size  $\Delta = (\delta x \delta y \delta z)^{\frac{1}{3}}$ , and the deformation term is related to the dissipation

$$\begin{aligned} \Phi \equiv \tau \cdot \nabla \mathbf{u} &\equiv \mu \left( 2(\text{def} \mathbf{u}) \cdot (\text{def} \mathbf{u}) - \frac{2}{3} (\nabla \cdot \mathbf{u})^2 \right) \\ &= \mu \left[ 2 \left( \frac{\partial u}{\partial x} \right)^2 + 2 \left( \frac{\partial v}{\partial y} \right)^2 + 2 \left( \frac{\partial w}{\partial z} \right)^2 + \left( \frac{\partial u}{\partial y} + \frac{\partial v}{\partial x} \right)^2 + \left( \frac{\partial u}{\partial z} + \frac{\partial w}{\partial x} \right)^2 + \left( \frac{\partial v}{\partial z} + \frac{\partial w}{\partial y} \right)^2 - \frac{2}{3} \left( \frac{\partial u}{\partial x} + \frac{\partial v}{\partial y} + \frac{\partial w}{\partial z} \right)^2 \right] \end{aligned} \quad (6)$$

The key coefficient in this model is the Smagorinsky constant  $C_s$  which is the sub-grid scale model coefficient that is flow dependent and has been optimized over a range from 0.1 to 0.25 for various flow configurations. As reported in literatures, the Smagorinsky coefficient is not a universal constant. It should be noted that the optimization of  $C_s$  in numerical simulation is generally ad hoc [29]. It was found that good results with the Smagorinsky model can be observed when  $C_s = 0.1$  for channel flow [24, 25],  $C_s = 0.12$  for the flow around a bluff body [30],

$C_s=0.16$  for a mixing layer [29] and an indoor airflow with force convection [28], and for homogeneous isotropic turbulence [25, 26]  $C_s$  ranges from 0.17 to 0.20 [29]. Geurts et al. [31] concluded that  $C_s=0.1$  roughly corresponds to the averaged dynamic coefficient in the developed flow condition. Even though there are some suggested values of the Smagorinsky constant for various flow configurations, theoretical guidelines have never been provided [29].

It is therefore necessary to find the optimum value of  $C_s$  for each flow configuration. After detail investigation, it is found that  $C_s=0.12$  is the best value for the current configuration in this study. This was determined by comparison with experiments and later used without change. Even though the Smagorinsky model has some shortcomings, it is still widely used for a number of applications.

### 3.3. Numerical method

Figure 2 shows the schematic diagram of the computational domain used in the current study. The computational domain is  $20D \times 20D \times 80D$  for single and three jets and  $40D \times 40D \times 160D$  for the five jet configuration based on the center jet diameter. The domain consists of  $80 \times 80 \times 256$  grid points in the X, Y and Z directions respectively for all cases. It has been proven that this resolution is sufficient to describe the flow and concentration fields considering the accuracy and computation time. All numerical calculations in this study have been performed within a domain that is made up of rectangular meshes, each with its own rectilinear grid.

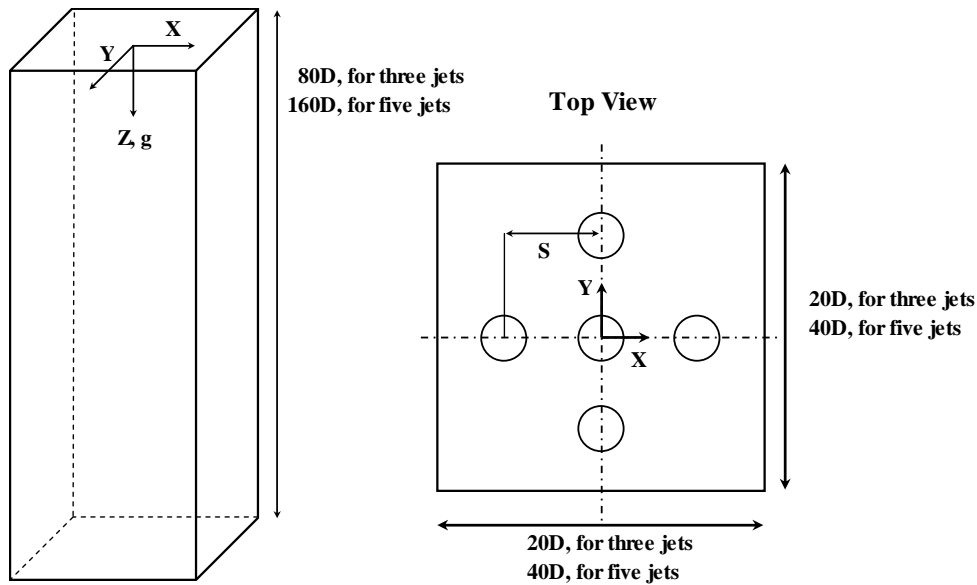


Figure 2: Schematic diagram of the computational domain and coordinates

## 4. Results and Discussion

In this section, the experimental and numerical results of passive scalar concentration field for single and three collinear water jets are presented. For more detailed analysis, extensive

numerical studies on five gas phase multiple turbulent jets are also performed. In this study, the Reynolds number of the jets is kept above  $10^4$  for sustaining the fully developed turbulence condition according to Dimotakis [22]. The parameters and properties of the turbulent jets are listed in Table 1.

Configurations		Working/Ambient Fluids	Jet Diameter (m)		Velocity (m/s)		Reynolds No.		Momentum Ratio	Separation Distance
			Center	Side	Center	Side	Center	Side	MR	S/D
Single	Water		0.0104		1.0		$1.16 \times 10^4$			
			0.0104		2.0		$2.33 \times 10^4$			
	Air		0.1		10.0		$6.45 \times 10^4$			
			0.1		20.0		$1.29 \times 10^5$			
3 Jets	S/D effect	Water/Water	0.0104	0.0104	1.0	1.0	$1.16 \times 10^4$	$1.16 \times 10^4$	1.00	3.66
			0.0104	0.0104	1.0	1.0	$1.16 \times 10^4$	$1.16 \times 10^4$	1.00	5.50
			0.0104	0.0104	1.0	1.0	$1.16 \times 10^4$	$1.16 \times 10^4$	1.00	7.33
	MR effect	Water/Water	0.0104	0.0104	1.0	2.0	$1.16 \times 10^4$	$2.33 \times 10^4$	0.25	3.66
			0.0104	0.0104	1.0	1.0	$1.16 \times 10^4$	$1.16 \times 10^4$	1.00	3.66
			0.0104	0.0104	2.0	1.0	$2.33 \times 10^4$	$1.16 \times 10^4$	4.00	3.66
	S/D effect	Methane & Air/ Water Vapor	0.05	0.1	40.4	24.0	$6.54 \times 10^4$	$1.55 \times 10^5$	0.39	4.0
			0.05	0.1	40.4	24.0	$6.54 \times 10^4$	$1.55 \times 10^5$	0.39	8.0
			0.05	0.1	40.4	24.0	$6.54 \times 10^4$	$1.55 \times 10^5$	0.39	12.0
	MR effect	Methane & Air/ Water Vapor	0.05	0.1	40.4	24.0	$6.54 \times 10^4$	$1.55 \times 10^5$	0.39	10.0
			0.05	0.1625	40.4	9.1	$6.54 \times 10^4$	$9.54 \times 10^4$	1.03	10.0
			0.05	0.2	40.4	6.0	$6.54 \times 10^4$	$7.75 \times 10^4$	1.57	10.0

**Table 1: The parameters and properties of turbulent jets in experiments and numerical simulations.**

#### 4.1. Single Jet

For validation, experiments and numerical simulations are performed on a single water jet. In addition, numerical simulations are conducted on a single gas jet as the basis of investigation of multiple turbulent gas jets. For a single jet, the working and ambient fluid are the same, thus no density effect is involved.

The mean concentrations along with the centerline of the longitudinal axis are plotted in Figure 3 (a), and scaled mean centerline concentrations are shown in Figure 3 (b) along with the results of current and previous experimental works [14, 15, 16, 17, 18, 20].

As shown in Figures 3 (a&b), the value of the mean centerline concentration  $C_c$  is constant in the potential core region and decays linearly with the streamwise distance after becoming fully developed, as expressed in equation (7).

$$\frac{C_o}{C_c} = \frac{1}{K_c} \left( \frac{Z - Z_o}{D} \right) \quad (7)$$



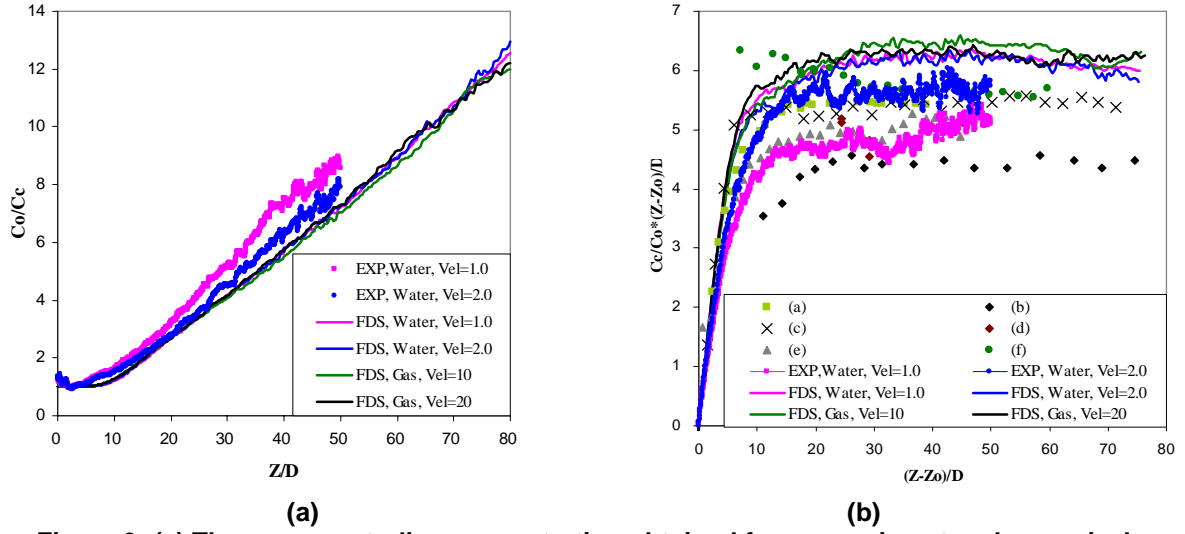


**Figure 3: (a) The mean centerline concentration obtained from experiment and numerical simulation for a single jet, and (b) comparison of current results with the previous works for the scaled mean centerline concentration, (a) Becker et al. [15], (b) Birch et al. [16], (c) Dahm [18], (d) Dowling and Dimotakis [20], (e) Lockwood and Moneib [17], (f) Wilson and Danckwerts [14].**

In equation (7),  $C_o$  is the injection concentration and  $D$  the jet diameter. The mean decay rate for the concentration  $K_c$  and the virtual origin  $Z_o$  for each condition are obtained according to equation (7) and listed in Table 2. In Figure 3 (b), the mean centerline concentration is scaled by  $(C_c / C_o)(Z - Z_o) / D$ , same as that used in Ref. [20], and plotted as a function of the distance from the jet virtual origin.

It is seen from Figure 3 (b) that the experimental results show good agreement with the previous work. The numerical simulation predicts a little longer potential core region up to  $Z/D=10$  and lower decay rate of the mean centerline concentration than the current and previous experimental results.

**Table 2: Decay rate  $K_c$  and virtual origin  $Z_o$  of a single turbulent jet obtained from experiment and numerical simulation.**

Jet phase	Exit velocity		Decay rate $K_c$	Virtual origin $Z_o$
Water Jet	Vel=1.0	Experiment	4.69	5.30d
		FDS	6.13	4.75d
	Vel=2.0	Experiment	5.59	4.70d
		FDS	6.06	4.94d
Air Jet	Vel=10	FDS	6.25	4.29d
	Vel=20	FDS	6.21	3.69d

However, the numerical prediction of the value of the decay constant  $K_c$  for all calculations is almost the same, and  $(C_c / C_o)(Z - Z_o) / D$  is nearly constant irrespective of the Reynolds number and the working fluids. Experimental measurements, on the other hand, show considerable scatter. The scatter in the experiments is attributed to the uncertainty in the initial conditions of the jet. Since the simulations have much less uncertainty, the curves are closer together. Nevertheless, the general similarity for a single turbulent jet is well established both experimentally and numerically [23].

The mean radial concentration profiles are plotted in Figure 4. Literature data are also plotted for comparison [15, 16, 18, 20]. As shown in the literature, the profiles appear self-similar and Gaussian-like for  $Z/D > 20$ . Clearly, FDS calculations agree well with the results in literature.

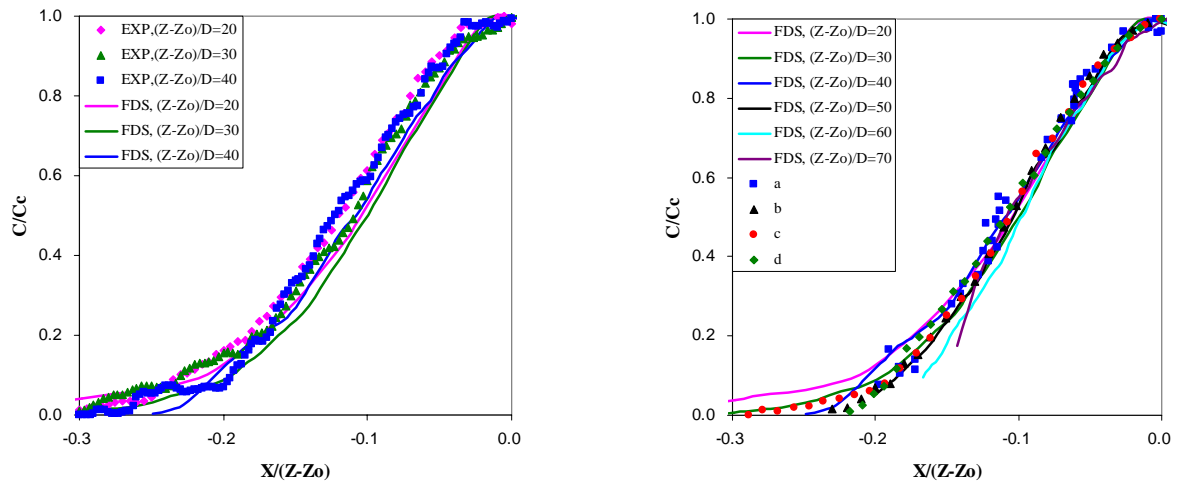


**Figure 4: The mean radial concentration profiles obtained from experiment and numerical simulation at exit velocity 1.0 m/s for a water single jet, and results of (a) Dowling and Dimotakis [20] (b) Becker et al. [15], (c) Birch et al. [16] and (d) Dahm [18].**

## 4.2. Multiple Jets

### 4.2.1. Water 3 Jets

To investigate the characteristics of mixing and concentration for multiple turbulent jets, experimental and numerical studies are performed on three collinear water jets. In this section, the effects of the separation distance and momentum ratio between jets are examined. The separation distance  $S/D$  and momentum ratio  $MR$  investigated in this study are listed in Table 1. For identification of the concentration of the central jet, salt water having the same properties as the side water jets is used as the central jet fluid in the numerical study.

#### *Separation Distance Effects*

The mean centerline concentration and scaled mean concentration of the central jet for three different separation distances with fixed jet velocity, 1.0-1.0-1.0 m/s, are plotted in Figure 5 (a) and (b). Single jet results are also shown for comparison. It is clearly observed that the linearity of the mean centerline concentration is broken and the value of  $(C_c / C_o)(Z - Z_o) / D$  is no

longer constant in multiple jets. The centerline concentration drops faster than the single jet due to enhanced mixing.

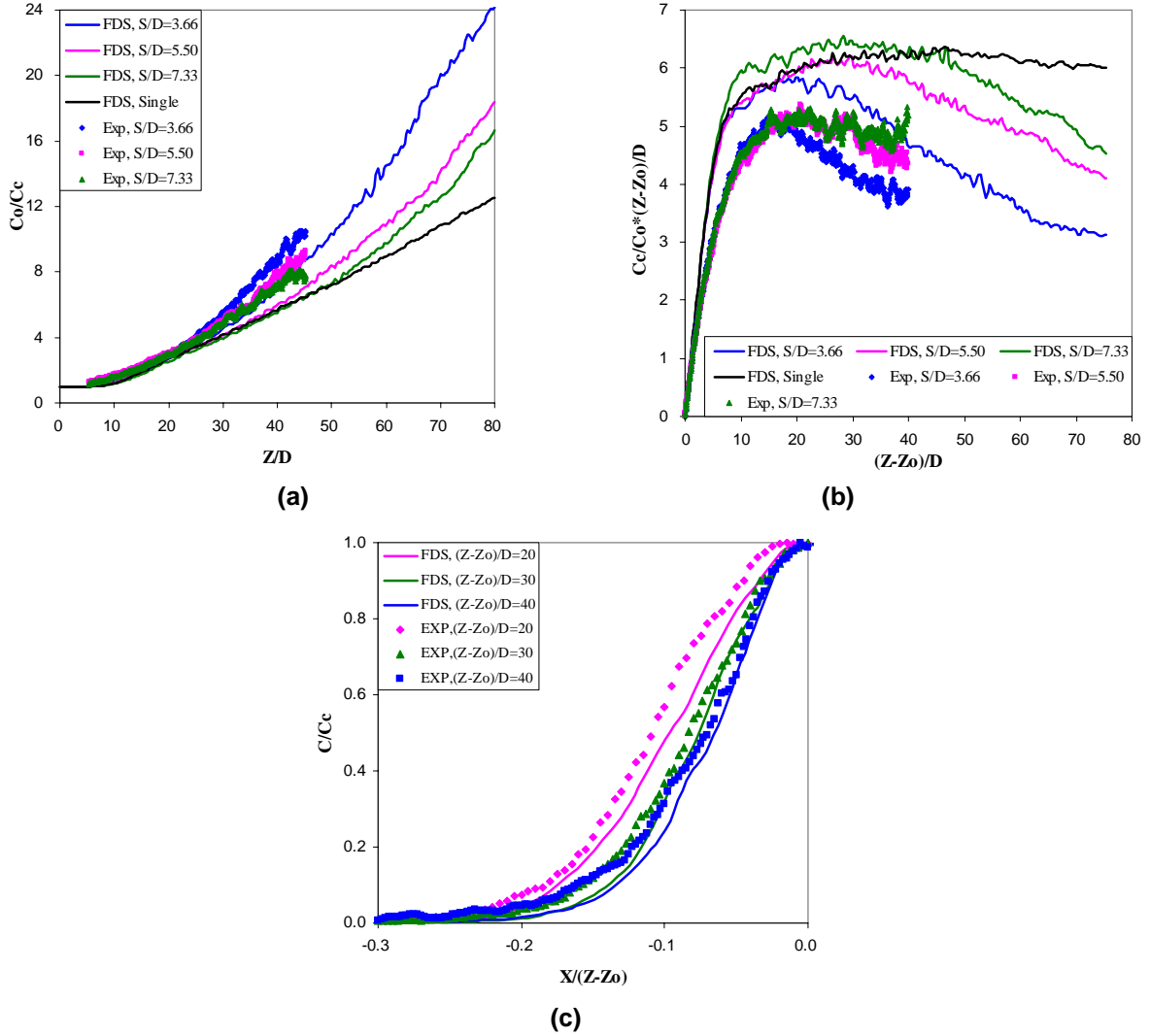


**Figure 5: Comparison of current experimental results with the numerical simulations for (a) mean centerline concentration, (b) scaled mean centerline concentration for  $S/D=3.66$ , 5.50 and 7.33 with jet velocity, 1.0-1.0-1.0 m/s and (c) mean radial concentration profiles for  $S/D=5.50$  with exit velocity, 1.0-1.0-1.0 m/s for three water jets.**

Thus, the general similarity is no longer valid in multiple jets. Even though using the concept of the virtual origin and scale factor  $(Z - Z_o)/D$  for the mean centerline concentration is not proper for the multiple jets, it is still useful to investigate that how the behavior of the multiple jets is different from a single jet. For this purpose, the virtual origin of a single jet is used for describing the value of  $(C_c/C_o)(Z - Z_o)/D$  in multiple jets.

As observed in Ref. [2, 7], Figure 5 (a) and (b) clearly show that the central jet initially follows the single jet path, and then deviates from the path after some distance. This deviation distance is the merge distance where the central jet begins to be affected by the side jets. From the merge

distance onward, the mean concentration of the central jet shows a completely different trend from that of a single jet. It is seen from Figure 5 (a) that the mean centerline concentration in the multiple jets decays faster than that of a single jet because of the exchange of momentum with side jets. It is also reported that multiple jets relatively entrain more surrounding fluid than a single jet, thus the mean centerline concentration decays faster in the multiple jet configuration [9, 13].

It is seen from Figure 5 (b) that the merge distance increases for larger jet spacing, which means that the separation distance between jets governs the distance after which the jets begin to interact [8, 11]. As shown in Figure 5 (c), the mean radial concentration profiles do not fall on a single curve for multiple jets and show a narrower width than a single jet. This can be attributed to the fact that the mutual interaction between jets creates a sub-atmospheric pressure region and in this region, the jets attract each other toward the centerline and thus the transverse transport rate decreases more than that of a single jet [10].

The mean centerline concentration of the central jet decays rapidly with decreasing the separation distance because a strong mutual entrainment and turbulent transport between jets starts earlier at shorter distance from the jet exits.

While there is some discrepancy between the experimental results and numerical predictions, the trend shows good agreement.

### ***Momentum Ratio Effects***

The effects of the momentum ratio between jets are investigated by changing the velocity of the jets while the diameter and flow rate of the jets are kept constant (see Table 1). Figure 6 shows the mean centerline concentration and the scaled mean centerline concentration of the central jet for three different momentum ratios  $MR$  of 0.25, 1.0 and 4.0 with fixed separation distance  $S/D=3.66$ . In this study, the momentum ratio is defined as the ratio of central jet momentum to side jet momentum.

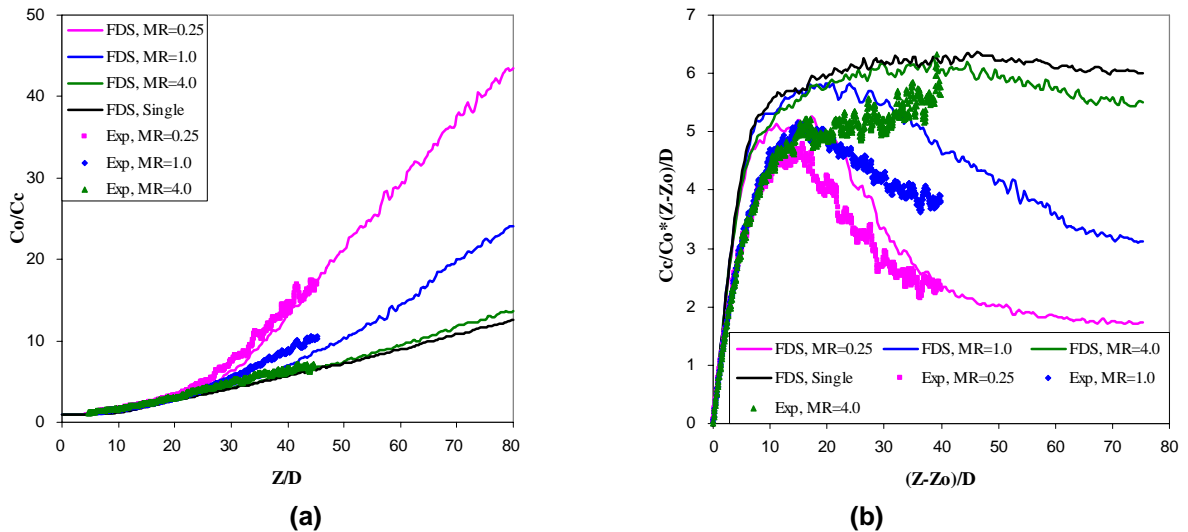


**Figure 6: Comparison of current experimental results with the numerical simulations for (a) mean centerline concentration and (b) scaled mean centerline concentration for  $MR=0.25, 1.0$  and  $4.0$  with separation distance  $S/D=3.66$  in three water jets.**

As shown in Figure 6, numerical predictions are in very good agreement with the experimental results. The discrepancy in the scaled mean concentration is observed between experiments and numerical prediction, because of the sensitivity of the scale factor  $(Z - Z_o)/D$  to the virtual origin. As stated before, the virtual origin of a single jet was used.

It is clearly observed that the mean centerline concentration of the central jet decays rapidly with decrease of the momentum ratio (increase the momentum of the side jet). The mean centerline concentration deviates quite rapidly from a single jet for  $MR=0.25$  case. An explanation could be that the entrainment of the ambient fluid into the side jets is enhanced due to their high momentum, and the side jets also entrain the central jet fluid again because of their higher momentum than the central jets. Thus, the central jet decays rapidly due to mixing with the side jets that have enhanced entrainment of the ambient fluid. This is important from the combustion point-of-view. Assume that the side jets are air, the central jet is fuel, and the ambient fluid is combustion products. Then, the entrainment of the central jet into the side jets will start combustion early before appropriate dilution – an undesirable consequence. On the other hand, if both the side and the central jets are appropriately diluted by the ambient fluid due to the high momentum of the side jets, then it is a desirable consequence.

The behavior of the mean centerline concentration of the central jet approaches that of the single jet at high momentum ratio  $MR=4.0$ . This can be attributed to the fact that the central jet having higher momentum is better able to penetrate into the side jets having lower momentum. Thus, the side jets are merged rapidly into the central jet. As a result, the multiple jets act like a single jet.

#### 4.2.2. Gas-phase Five Jets (Fuel & Oxidizer jets)

In this section, methane and normal air are used as a fuel and oxidizer, respectively. The central fuel jet is of 0.05 m diameter and the diameter of the four side oxidizer jets is varied to maintain the same flow rate and the overall equivalence ratio of 1.0 for all cases.

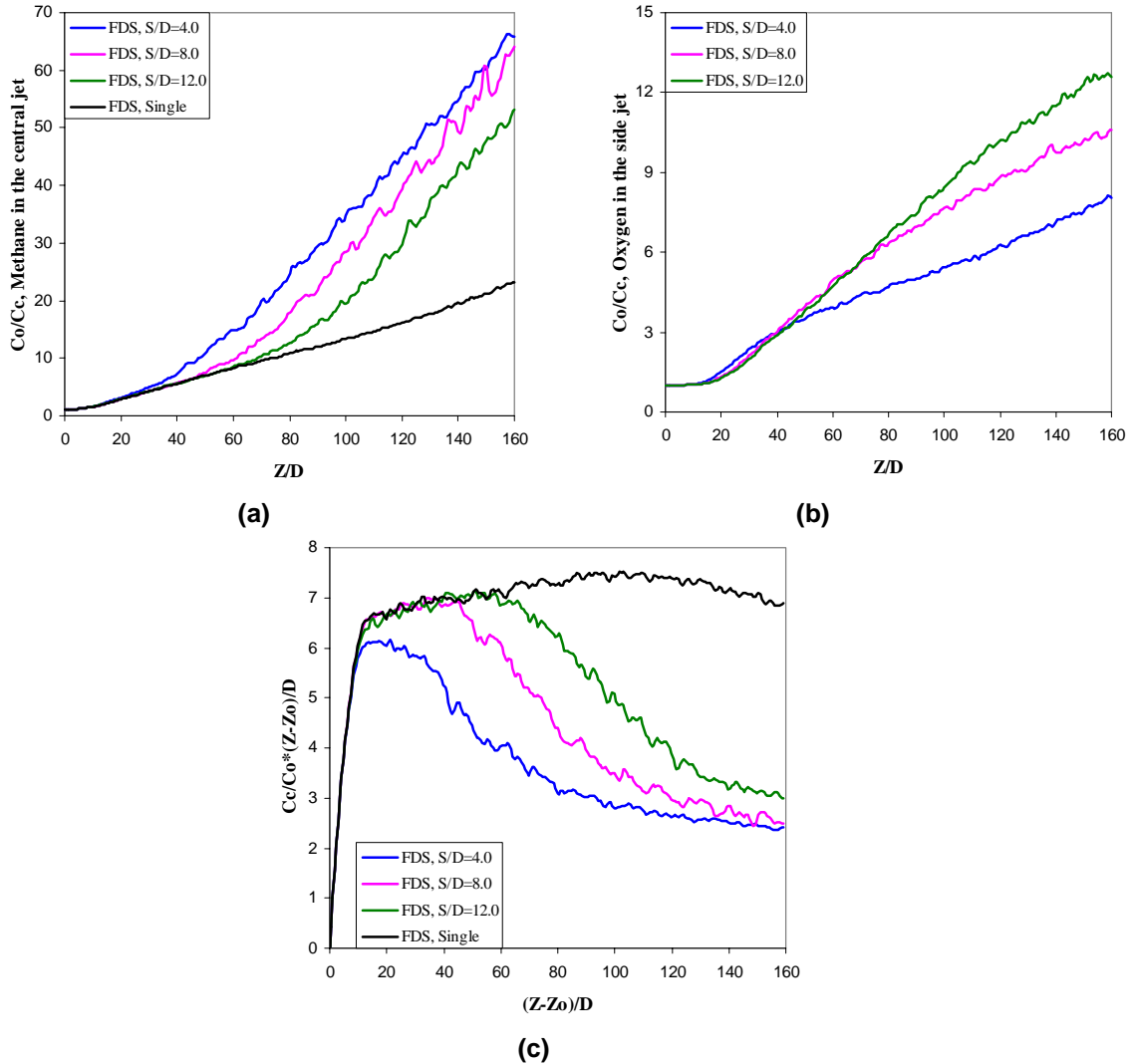
There are two available sources of jet dilution – one the ambient fluid (combustion products) and the other the jet fluids. For the current configuration, it is desirable that the jets are diluted by the entrainment of the ambient fluid and not by the other jets for achieving the homogeneous combustions. Therefore, it is important to identify the dilution source of the jets. For this purpose, methane and normal air are used as fuel and oxidizer, respectively, and water vapor is used as the ambient fluid. Thus, it is easy to investigate the dilution sources and mixing pattern between jets. It is noted that the background species cannot participate in the reaction except as a diluent in the FDS [36].

Numerical simulation for the configuration of a central jet (fuel) surrounded by four equidistant oxidizer jets are carried out for Reynolds number  $6.5 \times 10^4$  of the central jet. The separation distance is varied as  $S/D=4.0, 8.0, 12$  and the momentum ratio  $MR=0.39, 1.03$  and  $1.57$ .

#### *Separation Distance Effects*

The mean centerline concentration of the central (fuel) jet, side (oxidizer) jet and scaled mean centerline concentration of the central jet for three different separation distances with jet momentum ratio  $MR=0.39$  in the five multiple jet configuration are shown in Figure 7. For more detailed analysis, the mean concentrations of oxygen in the central (fuel) jet and methane in the side (oxidizer) jet are plotted in Figure 8, and the mean radial velocity profiles for  $S/D=4.0$  and  $12.0$  are plotted in Figure 9.

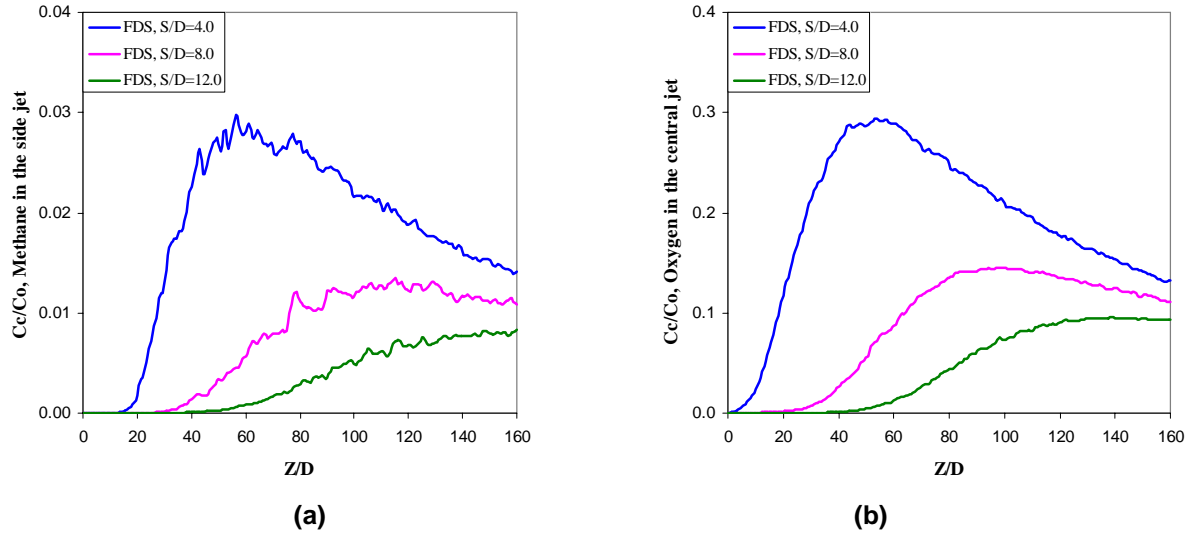
As shown in Figure 7, the behaviors of the mean centerline concentration of the central jet are similar to those of the three water jets. The central jet deviates from the single jet path after interacting with the side jets. It is also observed that the mean centerline concentration of the central jet decays rapidly with decreasing the separation distance and the behavior of the mean centerline concentration of the jets is close to that of a single jet at large separation distance.



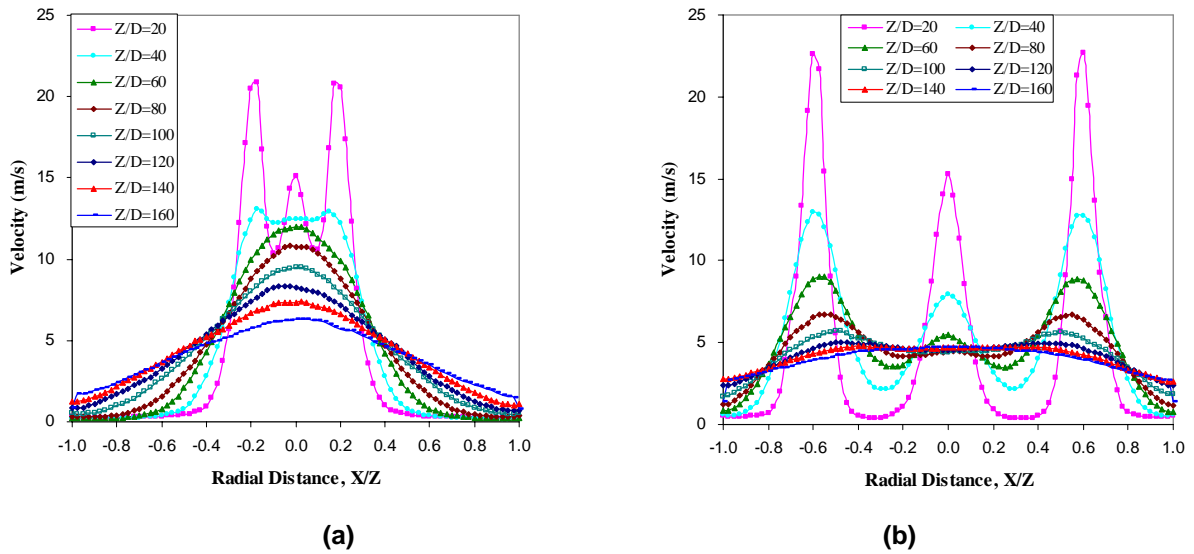
**Figure 7: Mean centerline concentration of the (a) central (fuel) jet, (b) side (oxidizer) jet and (c) scaled mean centerline concentration of the central jet for  $S/D=4.0$ , 8.0 and 12.0 with jet momentum ratio  $MR=0.39$  in five multiple jet configuration.**

Figure 8 shows lots of oxygen in the central (fuel) jet and some methane in the side (oxidizer) jets at a separation distance  $S/D=4.0$ . These concentrations begin to increase sharply near the jet exit and keep increasing up to  $Z/D=50$ , where the jet merging is completed, they then decrease far downstream. It is also observed from Figure 9 that the velocity profiles rapidly merge into the central jet after  $Z/D=40$  and the peak of velocity exists only at the centerline of the central jet for  $S/D=4.0$  case. This can be attributed the fact that there exists a strong interaction between jets due to rapid merging into one jet, thus, strong mixing of fuel and oxidizer occurs earlier. Therefore, for  $S/D=4.0$ , the central jet concentration decays faster by mixing with side jets in the

upstream region. After merging with the side jets, the jets act like a single jet. Consequently, the jets are diluted by the entrainment of the ambient after merging.



**Figure 8: Mean concentration of the (a) methane in the side (oxidizer) jet and (b) oxygen in the central (fuel) jet for  $S/D=4.0$ , 8.0 and 12.0 with jet momentum ratio  $MR=0.39$  in five multiple jets.**



**Figure 9: Mean velocity profiles for (a)  $S/D=4.0$ , and (b)  $S/D=12.0$  with jet momentum ratio  $MR=0.39$  in five multiple jet configuration.**

On the other hand, for large separation distance, the  $S/D=12.0$  case shows that much small amount of oxygen and methane exist in the central (fuel) and side (oxidizer) jets, respectively. It is observed that the concentration of methane and oxygen start to increase after  $Z/D=40$ , and then show quite flat profiles. Clearly, the mixing between jets is delayed by increasing the separation distance and meanwhile the jets are being diluted by the ambient fluid. This is a mechanism to control homogeneous combustion. Comparing the mean velocity profiles with the small separation distance, the  $S/D=4.0$  case, the peaks in the velocity profiles still exist near the centerline of the side jets up to  $Z/D=100$  and the velocity profiles become quite flat after merging. This indicates that there exists a lot of entrainment of the ambient fluid for large separation



distance. In other words, each jet follows the behavior of a single jet before merging and the concentration decays by the entrainment of the ambient fluid. After merging, all jets decay by mixing between jets and the entrainment of the ambient fluid. Similar trends were reported in Ref. [13] where multiple jets were shown to entrain more ambient fluid than a single jet, especially for larger separation distances.

Thus, it can be concluded that the entrainment of the ambient fluid is promoted before mixing between jets at large separation distances, while the mutual interaction between jets in the upstream region is enhanced for small separation distances. To get homogeneous combustion, the separation distance should be sufficiently large so that the jets are sufficiently diluted by the ambient fluid before they meet.

### ***Momentum Ratio Effects***

Figure 10 shows that the mean centerline concentration of the central, side jet and scaled mean centerline concentration of the central jet for three different momentum ratios with separation distance  $S/D=10.0$  in the five multiple jet configuration. The mean concentrations of oxygen in the central jet and methane in the side are plotted in Figure 11, and the mean velocity profiles for  $MR=0.39$  and  $1.57$  are shown in Figure 12.

It is seen from the Figure 10 that both of the central and the side jets show the larger decay rate of the mean centerline concentration at low momentum ratio  $MR=0.39$ , while relatively small amount of methane and oxygen exist in the side and central jet, respectively for  $MR=0.39$ , as shown in Figure 11. This indicates that both jets are more diluted by the entrainment of the ambient fluid than the high momentum ratio cases. It is clearly shown in Figure 12(a) that the peaks in the velocity profiles of the side jets still exist up to  $Z/D=80$  and overall level of the velocity profiles is larger than the large momentum ratio case  $MR=1.57$  because the side jets have higher momentum. Therefore, the side jets continue to entrain the ambient fluid, and as a result of mixing with side jets, the centerline concentration of the central jet also decays faster than the large momentum ratio case  $MR=1.57$ .

Figure 10 shows that the mean centerline concentration of the central and side jet decay slowly at high momentum ratio  $MR=1.57$ , and lots of oxygen in the central jet and methane in the side jet are found, as shown in Figure 11. This can be attributed the fact that the shear layer between jets grows stronger with increasing central jet momentum, and thus advection of scalar is promoted. As a result, mixing between jets is enhanced at high momentum ratios [37]. However, as shown in Figure 12 (b) that the peaks of the velocity profiles of the side jets decrease rapidly and merge into one jet with relatively lower level of the velocity than the  $MR=0.39$  case and at relatively shorter distance, about  $Z/D=60$ . The entrainment of the ambient fluid is less for the high momentum ratio case, as a result, less decay rate of the jet fluid concentrations.

Moderate momentum ratio  $MR=1.03$  shows similar trends in the mean centerline concentration of the central jet and methane concentration in the side jets as the  $MR=1.57$  case. The difference is the behavior of the side jets, which have intermediate momentum when compared with the momentum ratio  $MR=0.39$  and  $1.57$  cases.

Thus it may be concluded that the entrainment of the ambient fluid is promoted at low momentum ratio, while the mutual interaction between jets is enhanced at high momentum ratio. However, the overall behavior of the three momentum ratio cases is very similar; the difference between cases is not big due to the narrow range of the ratios. It should also be noted that the

mixing between jets starts at the same distance and at the same rate. However, it is observed that the entrainment of the ambient fluid is enhanced by decreasing the momentum ratio. Considering the small separation distance case, it is possible that the reaction occurs early and near the jet exit region with high momentum ratio because of enhanced mixing between jets. Therefore, lower momentum ratio between jets is preferable for small and moderate separation distance to promote the dilution by the ambient fluid before mixing between jets occurs, whereas higher momentum ratio is preferable for larger separation distance to enhance fuel dilution with ambient fluid before mixing between jets to achieve homogeneous combustion.

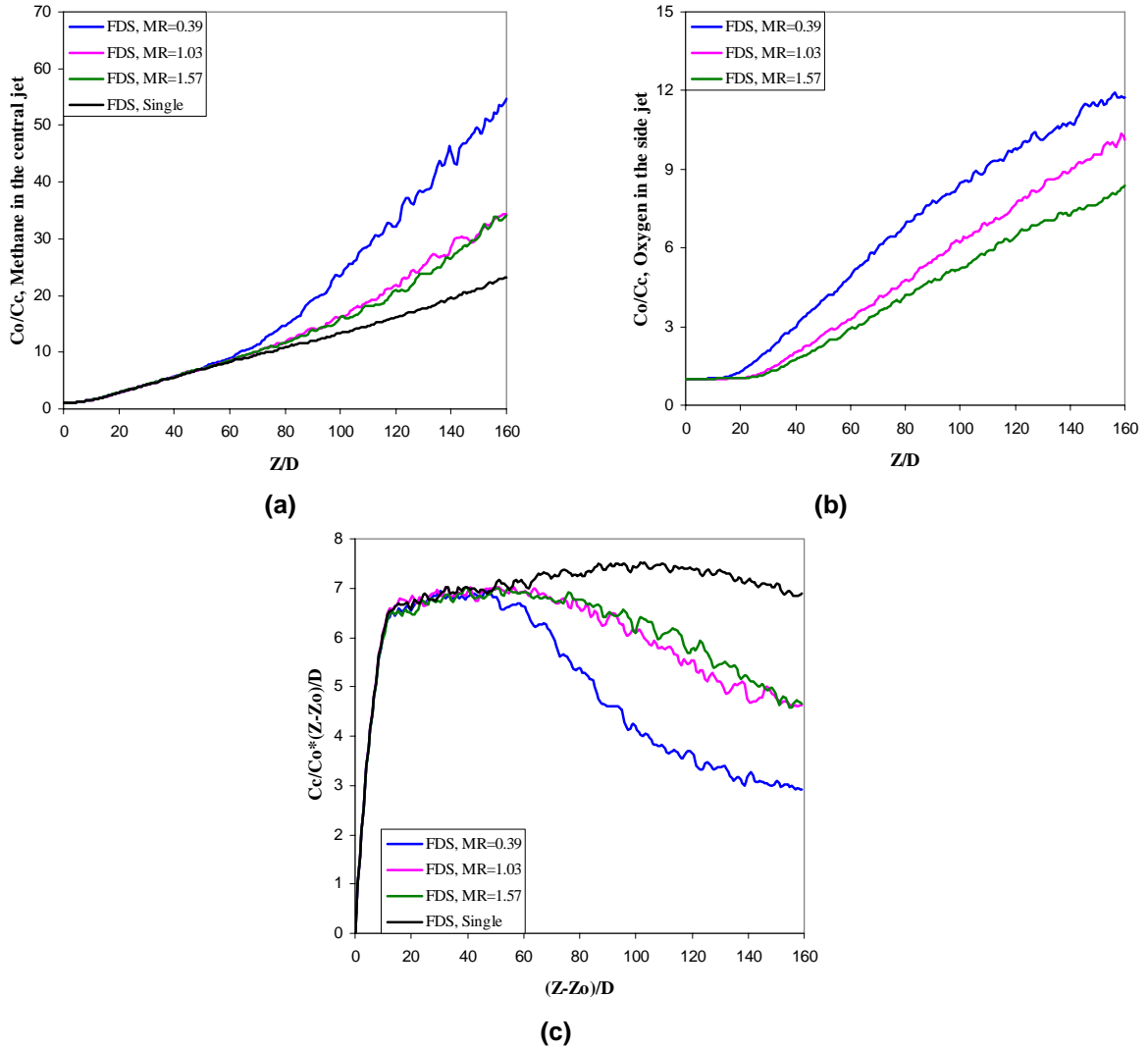
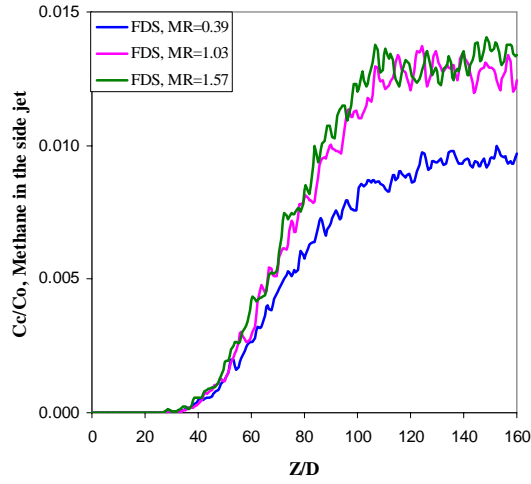
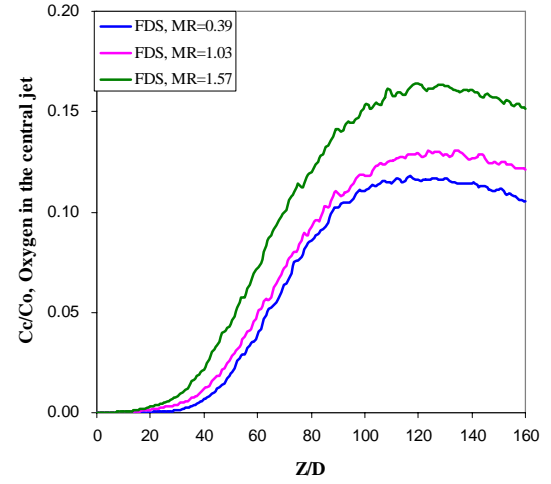


Figure 10: Mean centerline concentration of the (a) central (fuel) jet, (b) side (oxidizer) jet and (c) scaled mean centerline concentration of the central jet for  $MR=0.39$ ,  $1.03$  and  $1.57$  with jet separation distance  $S/D=10.0$  in five multiple jets.

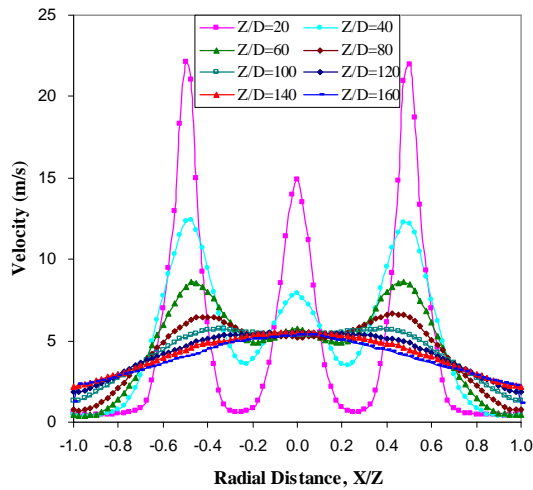


(a)

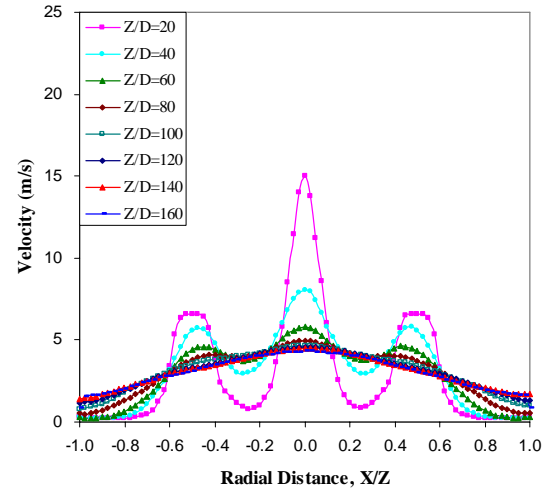


(b)

**Figure 11: Mean concentration of the (a) methane in the side (oxidizer) jet and (b) oxygen in the central (fuel) jet for  $MR=0.39$ ,  $1.03$  and  $1.57$  with jet separation distance  $S/D=10.0$  in five multiple jets.**



(a)



(b)

**Figure 12: Mean radial velocity profiles for (a)  $MR=0.39$  and (b)  $MR=1.57$  with jet separation distance  $S/D=10.0$  in five multiple jets.**

It is important to note that the longitudinal axis  $Z$  in Figure 10 (b) is normalized by the diameter of the center jet for the mean centerline concentration of the side jets; however the diameter of the side jets is varied to maintain the same flow rate and equivalence ratio for all cases, as mentioned before (see Table 1). This normalization is suitable for understanding the physical meaning at a given location (absolute position) along the longitudinal axis. It is observed that lower momentum ratio  $MR=0.39$  shows the largest decay rate of the side jets (Figure 10 (b)). In terms of the single jet theory, the concentration is proportional to the jet diameter at a certain absolute location. Thus a jet with a small diameter shows lower concentration than a jet with a large diameter at a given absolute distance from the jet exit. Figure 10 (b) coincides with the single jet theory because the mean centerline concentration of the side jets decays faster with

decreasing the momentum ratio which is equivalent to decreasing the side jet diameter. However, Figure 10 (b) shows that the mean centerline concentration of the side jets for all cases seems to decay less than that of a single jet. But, if the longitudinal axis  $Z$  is normalized by the actual side jet diameter as shown in Figure 13, it is observed that all cases show a higher decay rate than the single jet, as expected. Even though the high momentum ratio  $MR=1.57$  decays faster than other cases at relative position, the absolute distance needed to get the same concentration as the other cases is larger because of the large diameter.

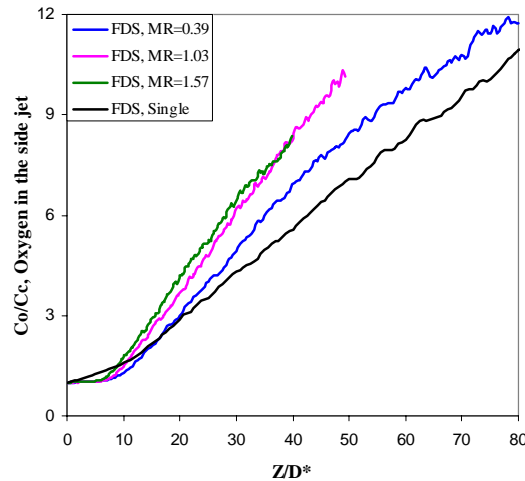


**Figure 13: Mean centerline concentration of the side jet for  $MR=0.39$ ,  $1.03$  and  $1.57$  with jet separation distance  $S/D=10$  in five multiple jet configuration. ( $D^*$  is the diameter of each side jet)**

## 5. Conclusion

Experimental and numerical investigations were performed on the mixing characteristics and the resulting concentration fields in unconfined and non-reacting multiple turbulent jets in terms of the control variables such as the separation distance and momentum ratio. The numerical results were found to be in good agreement with the experimental data for turbulent free jets.

The results of this study showed that mean centerline concentration decays faster in multiple jet configuration than a single jet because of the strong interactions between jets and enhanced entrainment of the ambient fluid. In multiple turbulent jets, the greater dilution in mean centerline concentration of the central (fuel) jet occurred at lower separation distance due to enhanced interaction and thus mixing between jets. For large separation distance, the entrainment of the ambient is promoted and mixing between jets is delayed to further downstream.

Decreasing the momentum ratio showed more dilution as a result of increased entrainment of the ambient fluid while high momentum ratio showed enhanced mixing between jets. However, it is possible that reaction may occur near the jet exit region due to strong mixing between jets for large momentum ratios and small separation distances.

In terms of achieving homogeneous combustion, the jets should be sufficiently diluted by the ambient fluid before mixing together. The mixing between jets should be delayed to some distance from the jet exit to enable sufficient dilution by the ambient fluid. Therefore, to achieve the homogeneous combustion, the separation distance should be kept sufficiently large and lower

momentum ratio between jets is preferable to promote the dilution by the ambient fluid before combustion occurs and to avoid early reaction.

## 6. Future Work

The situation of real industrial furnaces is quite different from the conditions in this study. The effects of the confinement and combustion must be considered. In addition, the effect of different density as a result of the combustion and recirculation with product gas also plays an important role in flow mixing and combustion process. Numerical study on confined and reacting jets in furnaces will be presented in the future.

## References

- [1] Becker, H. A., and Booth, B. D., *AIChE J.* 21:949 (1975).
- [2] Krothapalli A, Baganoff, D, Karamacheti K. Development and structure of a rectangular jet in a multiple jet configuration, *AIAA J.* 18(1980) 945–950.
- [3] Raghunathan, Reid IM. A study of Multiple jets, *AIAA J.* 19 (1981) 124 –127.
- [4] Okamoto, T., Yagita, M., Watanabe, A., and Kawamura, K., Interaction of Twin Turbulent Circular Jet, *Bull. JSME*, 28 (1985) 617–622.
- [5] E.W. Grandmaison, N.L. Zettler, Turbulent mixing in co-flowing plane jets, *Can. J. Chem. Eng.* 67 (1989) 889.
- [6] Wlezien, R. W., Nozzle Geometry Effects on Supersonic Jet Interaction, *AIAA J.* 27 (1989) 1361–1367.
- [7] Shu-Hao Chuang, Zuu-Chang Hong, Jhy-Horng Wang, Multiple-plane-jet turbulent mixing analysis via a kinetic theory approach, *International Journal for Numerical Methods in Fluids* 13 (1991) 83-107.
- [8] Moustafa, G. H., Experimental Investigation of High-Speed Twin Jets, *AIAA J.* 32 (1994) 2310–2322.
- [9] Steve LePera and Uri Vandsburger, Coupled multiple jet excitation, *Aerospace Sciences Meeting & Exhibit, 35th*, Reno, NV (1997).
- [10] A. A. Mostafa, M. M. Khalifa , E. A. Shabana, Experimental and numerical investigation of multiple rectangular jets, *Experimental Thermal and Fluid Science* 21 (2000) 171-178.
- [11] Wang, J., Priestman, G.H., Dongdi Wu, An analytical solution for incompressible flow through parallel multiple jets, *Transactions of the ASME. Journal of Fluids Engineering* 123 (2001) 407-410
- [12] Ibrahim Yimer, Henry A. Becker and E. W. Grandmaison, The strong-jet/weak-jet problem: new experiments and CFD, *Combustion and Flame* 124 (2001) 481-502.
- [13] C. H. Isaac Manohar, T. Sundararajan, V. Ramjee and S. Sasi Kumar, A numerical and experimental investigation of the interactions between a non-uniform planar array of incompressible free jets, *International Journal for Numerical Methods in Fluids* 44 (2004) 431–446.
- [14] R.A.M. Wilson and P.V. Danckwerts, Studies in turbulent mixing .2. a hot-air jet, *Chemical Engineering Science* 19 (1964).
- [15] H.A. Becker, H.C. Hottel, and G.C. Williams, The nozzle fluid concentration field of the round turbulent jet, *Journal of Fluid Mechanics* 30 (1967).
- [16] A.D. Birch, D.R. Brown, M.D. Dodson, and J.R. Thomas, The turbulent concentration field of a methane jet, *Journal of Fluid Mechanics* 88 (1978).
- [17] F.C. Lockwood and H.A. Moneib, Fluctuating temperature-measurements in a heated round free jet. *Combustion Science and Technology* 22 (1980).
- [18] W.A. Dahm, Experiments on entrainment, mixing, and chemical reactions in turbulent jets at high Schmidt number, Doctor of Philosophy Thesis, California Institute of Technology, 1985.
- [19] P.N. Papanicolaou and E.J. List, Statistical and spectral properties of tracer concentration in round buoyant jets, *International Journal of Heat and mass Transfer* 30 (1987).
- [20] D.R. Dowling and P.E. Dimotakis, Similarity of the concentration field of gas-phase turbulent jets, *Journal of Fluid Mechanics* 218 (1990).
- [21] E.W. Grandmaison, H.A. Becker, and N.L. Zettler, Scalar mixing in turbulent concentric round jets, *Canadian Journal of Chemical Engineering* 74 (1996).
- [22] Paul E. Dimotakis, The mixing transition in turbulent flows, *J. Fluid Mech.* 409 (2000).

- [23] C.L. Lubbers, G. Brethouwer, B.J. Boersma, Simulation of the mixing of a passive scalar in a round turbulent jet, *Fluid Dynamics Research* 28 (2001).
- [24] Deardorff J. W., A Three-dimensional numerical study of turbulent channel flow at large Reynolds numbers. *J fluid Mech* (1970) 41:453.
- [25] Mansour N. N., Moin P., Reynolds W. C., Ferziger J. H. In: Durst IF, et al., editors, *Turbulent shear flow*, Springer: New York (1979) 386.
- [26] Clark R. A., Ferziger J. H., Reynolds W. C., Evaluation of sub-grid scale models using an accurately simulated turbulent flow, *J Fluid Mech (Part 1)* (1979).
- [27] Moin P, Kim J., Numerical investigation of turbulent channel. *J Fluid Mech* (1982) 1118:341.
- [28] Mizutani K, Murakami S, Kato S, Mochida A., Study on influence of change of Smagorinsky constant. *Proceedings of the Architectural Institute of Japan Annual Meeting* (1991).
- [29] Kiyosi Horiuti, A proper velocity scale for modeling subgrid-scale eddy viscosities in large eddy simulation, *Physics of Fluids A: Fluid Dynamics* 5 (1993) 146-157.
- [30] Murakami S., Overview of turbulence models applied in CWE-1997, *J Wind EngInd Aerodyn* (1998).
- [31] Bernard J. Geurtsa, Jochen Fröhlich, A framework for predicting accuracy limitations in large-eddy simulation, *PHYSICS OF FLUIDS* 14 (2002).
- [32] Wüning J. A. and Wüning J. G., Flameless Oxidation To Reduce Thermal NO Formation, Vol. 23 of *Prog. Energy Combust. Sci*(1997) 81-94.
- [33] Katsuki M. and Hasegawa T., The Science and Technology of Combustion in Highly Preheated Air, In *Proceedings of the Twenty-Seventh(International) Symposium on Combustion*(1998) 3135.
- [34] Plessing T., Peters N., Wüning J.G., 1998, Laseroptical investigation of highly preheated combustion with strong exhaust gas recirculation, *28<sup>th</sup> International Symposium on Combustion, Boulder, Colo.* (1998) 3197-3204
- [35] De Joannon M., Langella G., Beretta F., Cavaliere A., Noviello C., Mild combustion : process features technological constrains, *Proceeding of the Mediterranean Symposium* (1999) 347-360.
- [36] K.B. McGrattan, H.R. Baum, R.G. Rehm, A. Hamins, G.P. Forney, Fire Dynamics Simulator—Technical References Guide, NIST Special Publication 1018, *National Institute of Standards and Technology* (20005).
- [37] A. Gokarn, F. Battaglia, R. O. Fox and J. C. Hill, Simulations of mixing for a confined co-flowing planar jet, *Computers & Fluids* 35 (2006) 1228-1238.